LAPORAN PENYELIDIKAN

THE DEVELOPMENT OF LOCAL SOLAR IRRADIANCE FOR OUTDOOR COMPUTER GRAPHICS RENDERING

VOT RMC 74135

PENYELIDIK:

DR. IBRAHIM BUSU

MOHD SHAHRIZAL SUNAR

PROF MADYA SARUDIN KARI

PROF MADYA DAUT DAMAN

PROF DR GHAZALI SULONG

PROF DR AZNI ZAIN-AHMED

PUSAT PENGURUSAN PENYELIDIKAN

UNIVERSITI TEKNOLOGI MALAYSIA

SESI 2003 / 2005

THE DEVELOPMENT OF LOCAL SOLAR IRRADIANCE FOR OUTDOOR COMPUTER GRAPHICS RENDERING

IRPA 2003 / 2005

KETUA PENYELIDIK:

DR. ISMAIL BIN MAT AMIN (JAN 2003 – JUNE 2005)

PENYELIDIK:

DR. IBRAHIM BUSU

MOHD SHAHRIZAL SUNAR

PROF MADYA SARUDIN KARI

PROF MADYA DAUT DAMAN

PROF DR GHAZALI SULONG

PROF DR AZNI ZAIN-AHMED

Faculty of Computer Science and Information System

Universiti Teknologi Malaysia

Skudai, Johor.

TEMPOH PENYELIDIKAN: JANUARY 2003 – JUNE 2005

VOT RMC 74135

PUSAT PENGURUSAN PENYELIDIKAN

UNIVERSITI TEKNOLOGI MALAYSIA

R & D DIRECTORY UTM

VOT:	74135
PROJECT TITLE:	THE DEVELOPMENT OF LOCAL SOLAR IRRADIANCE FOR OUTDOOR COMPUTER GRAPHICS RENDERING
HEAD OF RESEARCHERS:	DR. ISMAIL BIN MAT AMIN (JAN 2003 – JUNE 2005)
RESEARCHERS:	DR. IBRAHIM BUSU MOHD SHAHRIZAL SUNAR PROF MADYA SARUDIN KARI PROF MADYA DAUT DAMAN PROF DR GHAZALI SULONG PROF DR AZNI ZAIN AHMED
FACULTY:	FACULTY OF COMPUTER SCIENCE AND INFORMATION SYSTEM UNIVERSITI TEKNOLOGI MALAYSIA SKUDAI, JOHOR.
KEYWORDS:	ATMOSPHERIC MODEL, NUMERICAL MODELLING, SOLAR RADIATION, IMAGE SYNTHESIS
DATE OF COMPLETION:	JUNE 2005

TABLE OF CONTENTS

TABLE OF CONTENTS

ABSTRACT

Atmospheric effects are approximated by solving the light transfer equation, LTE, of a given viewing path. The resulting accumulated spectral energy (its visible band) arriving at the observer's eyes, defines the colour of the object currently on the line of sight. Due to the convenience of using a single rendering equation to solve the LTE for daylight sky and distant objects (aerial perspective), recent methods had opt for a similar kind of approach. Alas, the burden that the real-time calculation brings to the foil had forced these methods to make simplifications that were not in line with the actual world observation. Consequently, the results of these methods are laden with visual-errors. The two most common simplifications made were: i) assuming the atmosphere as a full-scattering medium only and ii) assuming a single density atmosphere profile. This research explored the possibility of replacing the real-time calculation involved in solving the LTE with an analytical-based approach. Hence, the two simplifications made by the previous real-time methods can be avoided. The model was implemented on top of a flight simulator prototype system since the requirements of such system match the objectives of this study. Results were verified against the actual images of the daylight skies. Comparison was also made with the previous methods' results to showcase the proposed model strengths and advantages over its peers.

ABSTRAK

Efek-efek atmosfera dikira dengan menyelesaikan formula pemindahan cahaya, LTE, untuk garis penglihatan yang diberi. Hasil terkumpul tenaga spektra (hanya untuk julat nampak) yang tiba di mata pemerhati akan menentukan warna terhadap objek yang sedang berada di hujung garis penglihatan. Oleh kerana ianya lebih senang jika menggunakan hanya satu formula rendering untuk langit dan objek-objek jauh (perspektif aerial), teknik-teknik terkini kebiasaannya memilih untuk mengaplikasikan pendekatan sebegini. Malangnya, beban pengiraan masa-nyata yang terpaksa dihadapi jika menggunakan pendekatan sebegini menyebabkan teknik-teknik terkini tersebut memperkenalkan ringkasan-ringkasan yang tidak selari dengan pemerhatian dunia sebenar. Akibatnya, hasil-hasil daripada teknik-teknik tersebut dipenuhi dengan pelbagai kesilapan visual. Dua ringkasan yang sering digunakan ialah: i) menganggap atmosfera sebagai medium penyesaran sahaja dan ii) menganggap ketumpatan atmosfera bumi sebagai sama sahaja di semua aras. Penyelidikan ini bertujuan untuk mengkaji kemungkinan untuk menggantikan pengiraan masa-nyata yang telibat semasa menyelesaikan LTE dengan suatu pendekatan analitikal. Hasilnya, dua ringkasan yang disebut di atas mampu untuk dielakkan. Model yang terhasil telah diimplementasi di dalam sebuah sistem prototaip untuk simulasi penerbangan disebabkan keperluan-keperluan untuk sistem tersebut amat padan dengan objektif-objektif penyelidikan ini. Hasil-hasil seterusnya diverifikasikan dengan gambar-gambar sebenar lelangit siang. Perbandingan juga dilakukan dengan teknik-teknik terdahulu untuk membuktikan kekuatan serta kelebihan model yang dibangunkan.

CHAPTER 1

INTRODUCTION

1.1 Introduction

The term "*atmospheric effects on both sky and distant objects"* is used to signify the observable state of appearance of these two entities: i) daylight sky and ii) distant objects, due to the *extinction* and *in scattering* of light on a given line of sight (*viewing path*). In scattering adds light whilst extinction removes light from the given viewing path. The light extinction can be further divided into two subsets: i) *out scattering* and ii) *absorption*. Both are equally important in defining the volume of attenuated light from the given viewing path.

Nevertheless, all of the previous works done on modelling the real-time light interactions with the *participating medium* had deliberately excluded absorption from their extinction model. This is one of the two most common simplifications made by the previous methods in order to remain feasible for a real-time implementation. They justified the exclusion based on the finding by (Haltrin, 1996) whereas absorption of the visible light is negligible except for the ozone layer. Hence, the layers below the ozone layer can be treated as a full scattering-only medium. The exclusion is not surprising since these works are more ontogenetic-based than teleological; the two polar extremes of modelling as explained by (Barr, 1991). The first approach (ontogenetic) is visually-driven: by developing methods that may or may not conform to the physics of light

transfer but are guaranteed to give visually-good results whilst the second approach (teleological) is far more rigorous: by developing a computational implementation of the mathematical models taken from the scientific literatures. The results are guaranteed to be visually correct but sometimes it can be the case of over-modelling (Fournier, 1989). Unnecessary complex mathematical models were used even though they may not improve the visual results significantly to justify their inclusion at the first place.

(Musgrave, 1993) argued that when developing realistic landscape imaging, the work should be image-driven.

"...the measure of success of the models developed here has generally been visual appearance rather than, for instance, scientific veracity. Thus the emphasis has been more on the creation of realistic-looking pictures, than on the construction of mathematically or physically corrects models."

(Musgrave, 1993)

This work, albeit being image-driven, never neglected the physical accuracy of the models chosen. Physically correct models will, without any doubt, produces visually correct results. Thus, the aim should be on matching the physically correct mathematical models as closely as possible, without sacrificing the interactive performance. (Preetham et al., 1999) agreed with this side of the view.

"*Our approach is motivated by the desire to generate images of real terrain, so we pay attention to maintain a physically-based radiometry, and use input parameters that are readily available to computer graphics researchers. We feel that current approaches are either far too general or expensive to be easily used, or include too many simplifications to generate a sufficiently realistic appearance.*"

(Preetham et al., 1999)

The two quotes above were inserted in this report to prove the point that the debate between the two extremes of modelling still remains as a highly subjective

matter. Either one or a combination of both is permissible, as long as the justifications behind it made are logical.

As (Blinn, 1982) had noted, the task of modelling the light scattering has two distinct problems: i) devising the geometric models of the Earth's atmosphere exponential density distributions, upon which the optical density of the light scattering depends, and ii) integrating both the extinction and in scattering of light over arbitrary viewing paths through these density distributions.

Most of the previous works sidestepped the first problem by assuming the Earth's atmosphere density as constant. This assumption limited the possible rendering of the daylight skies to the ones observed from the ground level only. The second problem, the solving of the light transfer equation (LTE) of a given viewing path is also inadequately dealt with. These real-time methods: i) excluded absorption from their version of the LTE's extinction part and ii) assumed a single density profile for the Earth's atmosphere.

This report presents a significant and original analytical-based approach to replace the real-time atmospheric colour contribution calculation in the original LTE. As a result, two key models were developed: i) an exponential atmospheric colour contribution model and ii) a single rendering equation model to render both sky and distant objects.

The first model (the exponential atmospheric colour contribution model) interpolates the five computed reference layers' sky colour distributions against the observer's current altitude to obtain the current layer's sky colour distribution. The sky dome endpoint currently intersected by or associated with the viewing path is assigned as its atmospheric colour contribution value. Typically, this value is calculated in real time since it is dependent on the arbitrary optical depth and angular angle of the viewing path from the sun. This report proved that the proposed exponential atmospheric colour contribution model does consider both parameters in its calculation hence maintaining its legitimacy.

The second model (the single rendering equation model) was based on the Beer's Law (Considine, 1976). Using the calculated transparency value together with the first model's output, the final pixel/vertex colour of the current viewing path is obtained.

Both models were successfully integrated into a single pixel/vertex-based shader program. A prototype of the shader was then developed to test the algorithms feasibility in a real-time flight simulator domain.

1.2 Research Background

Both daylight sky colour and aerial perspective effects (witnessed on the appearance of distant objects) are caused by the exact same process: the light interactions with the participating medium on a given viewing path. These interactions are modelled using the light transfer equation, LTE. Consequently, both phenomenons shared most of the previous works done on the topic of modelling the LTE through the Earth's atmosphere.

Nevertheless, slight dissimilarities exist between those two phenomenons (Preetham et al, 1999). The dissimilarities are: i) the sky dome endpoints are defined as a fixed unit of direction from the camera whilst a distant object is defined as an arbitrary unit of direction from the camera and ii) the optical depth for each endpoint from the camera are fixed while the optical depth for a randomly positioned distant object from the camera may varies unreservedly. This is by assuming the camera (observer) as the permanent centre of the universe.

Unlike a distant object, a sky dome's endpoint has no rigid body. It simply is just an imaginary point on the sky dome. This explains why an endpoint has a fixed set of zenith and azimuth angles with a constant optical depth value. Just think of the sky dome as a hemispherical structure that "follows" the camera (positioned at its centre) movement. Meanwhile, distant objects such as terrains, buildings,

vegetations et cetera are rigid bodies. If the camera is repositioned, the object's zenith and azimuth angles will inevitably change, so does the viewing path's optical depth.

1.2.1 Previous Works on Solving the LTE

Previous works on solving the LTE are divided into two categories: i) real-time and ii) offline image synthesis. Simulation-based and aerial perspective-based methods belong to the first category (real-time image synthesis) whilst analytical-based methods belong to the second category (offline image synthesis).

Simulation-based works such as (Klassen, 1987); (Kaneda et al, 1991); and (Nishita et al, 1996) were only concerned on solving the light scattering problem to simulate the daylight sky colour. (Klassen, 1987) used a planar layer atmospheric model and single scattering to simulate the daylight sky colour. (Kaneda et al. 1991) employed a similar simulation using a spherical atmosphere with air density changing exponentially with altitude. (Nishita et al., 1996) introduced multiple scattering and developed their method to visualise the Earth's atmosphere from space. All of these methods required a lengthy simulation for a given sky condition, but have the advantage of working with arbitrarily complex atmospheric conditions.

Analytical-based works such as (Kittler (CIE, 1994); (Moon and Spencer CIE, 1994); (Perez et al., 1993); and (Preetham et al., 1999)) were developed for the purpose of offline image synthesis. These methods are parametric in nature and were based on the fits of simulated or measured data. CIE organized the International Daylight Measurement Program (IDMP) to collect worldwide information (measured data) on the daylight availability. As for the simulated data source, several solar spectral parametric models are available for usage, such as SMARTS2 (Gueymard, 1995) and SPCTRAL2 (Bird and Riordan, 1986). These models can be used to simulate the daylight sky irradiance/illuminance distribution with a varying degree of success.

Aerial perspective-based works such as (Hoffman and Preetham, 2002 and Nielsen, 2003) can be assumed as a successor to the simulation-based works. These methods employed a single rendering equation, implemented as a pixel/vertex-based shader, for both sky and distant objects. The differences between those two were their initial colour and distance (optical depth) from the camera. The sky initial colour is black whilst for the distant objects; each has its own respective initial colour. The obvious advantage is the ability to simulate the atmospheric effects on both sky and distant objects using a single pixel/vertex-based equation. This nicely complements the modern graphic hardware-rendering pipeline. (Hoffman and Preetham, 2002) developed a single pixel/vertex-based shader for each three-colour channel (RGB). The model takes into account both the extinction (minus absorption) and in scattering part of the light transfers equation. (Nielsen, 2003) extended (Hoffman and Preetham's, 2002) model to consider a non-constant density atmosphere. (Nielsen's, 2003) model also corrected some of the visual flaws inherited from the original (Hoffman and Preetham's, 2002) model, albeit using less than accurate solving methods.

1.2.2 Previous Works on Visualizing the Subsequent Spectral Results

Spectral rendering describes the process of converting the spectral distribution into the RGB-colour space for computer display purposes. Colour space conversion issues are govern by the International Commission of Illumination, abbreviated from its French title: *Commission Internationale de l'Eclairage* (CIE).

1.3 Research Motivation

These are the two factors that motivate this research: i) inaccurate extinction model employed by the previous real-time methods and i) incorrect assumption made by the previous real-time methods on the Earth's atmosphere density.

The first motivating factor stemmed from the fact that most formulas used in the previous real-time methods were the product of aggressive simplifications made towards their equivalent mathematical models taken from the scientific literatures. Simulation-based works such as (Klassen, 1987), (Kaneda et al., 1991) and (Nishita et al., 1996) focused only on tackling the light scattering problem; ignoring absorption contribution completely. This leads to incorrect results since the ozone absorption is the key reason why the zenith sky remains blue during sunrise and sunset (Minnaert, 1954). The aerial perspective methods such as (Hoffman and Preetham, 2002) and (Nielsen, 2003) excluded absorption from their final shader implementation; considering only Rayleigh and Mie out scattering coefficients for the LTE extinction part.

The second motivating factor stemmed from the need to simulate a correct sky colour distribution with respect to the flight altitude. Previous methods, except for (Nielsen's, 2003) and (Musgrave's, 1993), all assumed a single density profile to represent the Earth's atmosphere. However, actual measurement done by (McCartney, 1976) revealed that the Earth's atmosphere density interpolates exponentially with the altitude.

1.4 Problem Statement

Current real-time approaches are burdened by the weight of the real-time calculations involved when solving the light transfer equation, LTE, on a given viewing path. In order to maintain their real-time feasibility, these methods made various simplifications towards their version of the LTE. The two most common simplifications made were: i) treating the Earth's atmosphere as a full-scattering medium by ignoring absorption contribution and ii) assuming a single density profile to represent the Earth's atmosphere.

1.5 Goal

This research is intended to explore the possibility of using an analytical-based approach to replace the traditional real-time calculations involved when solving the LTE of a given viewing path. The resulting algorithms were implemented as a pixel/vertex-based shader; tested on a flight simulator prototype system with terrain and a hemispherical sky dome rendering. The results were then evaluated against real images of the daylight skies; selected purposely to demonstrate the developed model properties. The proposed model performance was also compared with the previous methods to demonstrate its strengths and advantages over its peers.

1.6 Research Objectives

(i) Construct a profile of the Earth's general atmosphere up to 30km.

(ii) Produce a sky colour (spectral irradiance) distribution map for each possible sky condition.

(iii) Fit each map to a chosen parametric function to produce a look-up table relating the (Perez et al's, 1993) five parameters with these three inputs: i) reference layer altitude, ii) turbidity and iii) sun position.

(iv) Develop an exponential atmosphere colour contribution model based on the above look-up table.

(v) Develop a single rendering equation, implemented as a pixel/vertex-based shader, to simulate the atmospheric effects on each vertex or pixel passed on to the OpenGL API.

1.7 Research Scopes

(i) This research is only concern on simulating the daylight clear (cloud-free) skies.

(ii) The term "*general atmosphere*" is employed here since the data used are not from a specific site hence the physical veracity of the developed atmospheric profile cannot be guaranteed.

(iii) The pixel/vertex-based shader is only guaranteed to work under the given system specifications.

1.8 Research Contributions

This research contributes to the following aspects:

(i) By considering the absorption of light in the LTE's extinction part, visual errors caused by the exclusion (Minnaert, 1954) can be avoided.

(ii) By treating the Earth's atmosphere density as an exponential function of altitude, the sky colour distribution effects exhibited when observed from a higher altitude can be captured correctly.

This work is considered as an applied research thus benefiting the following areas:

(i) Computer Games – A computationally efficient method will enable low-end computer to render both sky and aerial perspective effects in an acceptable interactive frame rate. Flight simulator game reaps the most benefits.

(ii) Military/Airline Industry – Help familiarize beginner pilot with the various sky conditions (turbidity level and time setting) as expected to be observed in the real world. Aerial perspective effects helps pilot to judge both scale and distance properly.

(iii) Tourism – Virtual tourism via the "*fly-by*" method.

1.9 Organization of Report

This report is consisted of six chapters as follows:

Chapter 1 briefly introduces the topic of atmospheric effects rendering and its related research background. The research motivations and the problem statements are also defined. Goal, objectives and scopes of research are stated clearly. Finally, research contributions are listed and discussed.

Chapter 2 conducts a review to the topic of atmospheric effects rendering, consisting of concise explanations on: i) the theory of the light transfer and ii) the basic problems of the atmospheric effects rendering. The previous works on solving the LTE through the Earth's atmosphere are also reviewed and compared comprehensively.

Chapter 3 presents the methodology of this research. It consists of the following procedures: i) building a general atmospheric profile (up to 30km); ii) producing the all-sky (spectral irradiance) maps for each reference layer; iii) converting the all-sky (spectral irradiance) maps' unit to Yxy; iv) producing a look-up table by fitting the all-sky (Yxy) maps to a parametric function; v) developing an exponential atmospheric colour contribution model; and vi) developing a pixel/vertex-based rendering equation (RGB).

Chapter 4 reports on the implementation of the proposed methodology. The methodology is designed to be implemented modularly by two phases: i) pre-processing (offline) and ii) run-time processing (real-time). This chapter illustrates the workflow of these modules using pseudocodes and diagrams whenever deemed as necessary.

Chapter 5 shows the test results; each with its own complete individual analysis. The advantages, constraints and drawbacks of the proposed model are also discussed in this chapter.

Chapter 6 summarizes and concludes this study. It also outlines the topics for future work.

CHAPTER 2

LITERATURE REVIEW

2.1 Introduction

This chapter reviews the relevant literature on the topic of atmospheric effects rendering through the Earth's atmosphere. The theory of the light transfer is explained first. Important terms such as optical depth, visibility and viewing path are described here in this section. In addition, the explanation on the causes of the daylight sky colour and aerial perspective effects are also given.

Next, the basic problems of rendering these atmospheric effects on both sky and distant objects are examined thoroughly. Issues regarding the conversion of spectral distribution to RGB are also discussed here. Lastly, all the significant works on rendering the atmospheric effects for the past twenty years are reviewed. These methods are grouped according to the classification made by Preetham in his SIGGRAPH 2003 course notes (Preetham, 2003). These methods are then compared side-by-side in term of their capability in fulfilling the flight simulator domain requirements.

2.2 Light Transport in the Atmosphere

Before delving much further in the discussion, it is important to first understand the geometrical parameters used in this report to represent the celestial objects on the scene, including the sun and the sky dome endpoints. The geometrical parameters representing the sun trajectory are described in Figure 2.1. The three parameters are: i) solar elevation angle, hs, ii) solar zenith angle, θ_s and iii) solar azimuth angle, γ_s. Azimuth angle is calculated clockwise from north. These parameters can also used to represent the sky dome endpoints' location.

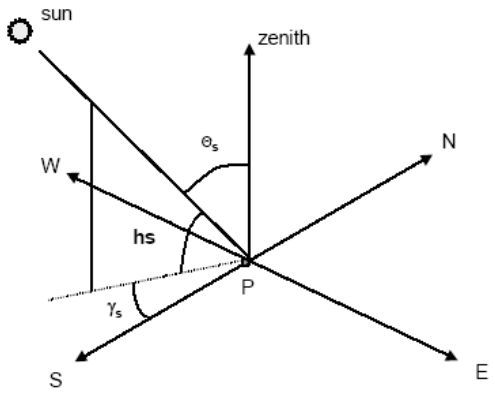

Figure 2.1 Geometrical parameters of the solar trajectory.

Now, let's move on to the discussion on light. Light is the visible band of the incoming electromagnetic spectrum (see Figure 2.2). Light originates from the sun and enters the Earth's atmosphere in almost a parallel manner due to the vast distance covered (see Figure 2.3). Light may enter the camera's viewing path as a primary or a secondary-sourced of energy. Primary refers to the light coming directly from the sun; being scattered only once before entering the viewing path. Secondary refers to the light that had been multiply-scattered by the atmosphere before entering the viewing path.

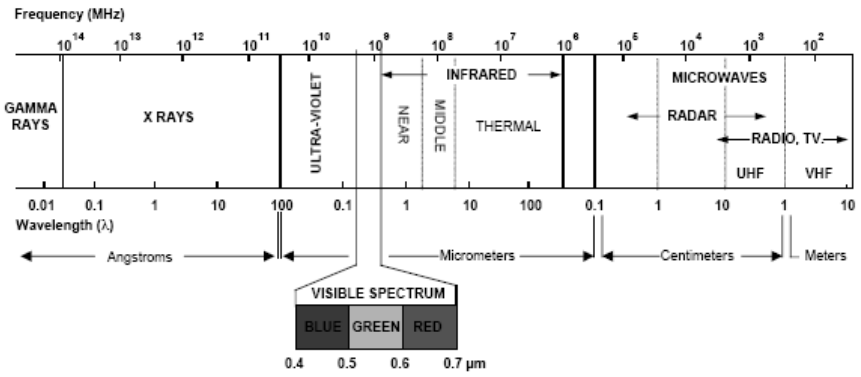

Figure 2.2 Electromagnetic spectrum with the visible band highlighted.

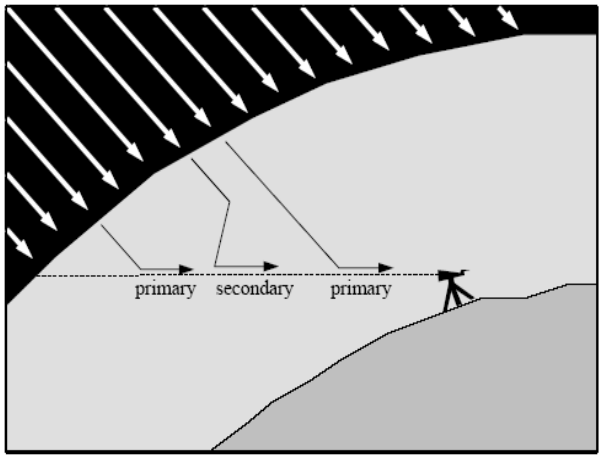

Figure 2.3 Earth receives an almost parallel illumination from the sun.

The viewing path, also known as the optical path, is an imaginary straight line connecting the observer's eyes (the camera) and the object currently on the line of sight. In Figure 2.3, the object refers to a sky dome endpoint. The object may also refer to the surface of a distant object.

The viewing path can be further divided into similar-sized sub elements; each with its own individual scattering coefficient value. Scattering coefficient is defined as the amount of light removed from a viewing path by scattering at a particular sub

element. The integral of the scattering coefficient of all sub elements on the given viewing path is represented by a dimensionless unit: optical depth. This dimensionless value will play an important role in defining the sky colour distribution. Further explanation on the influence of optical depth on the sky colour is given in Section 2.2.5.

The atmospheric contents, either molecules or particles that interact with the incoming light are termed as the participating medium. These interactions are described next.

2.2.1 Rayleigh Scattering

A particle that is smaller (usually less than 1/10) than the wavelength of light exhibits Rayleigh scattering (Rayleigh, 1871). The amount of scattering for such particles is inversely proportional to the 4^{th} power of the wavelength. These particles scatter equally in both forward and backward directions (see Figure 2.4). Molecules fall into this category, thus scattering by molecules can be described as a pure Rayleigh scattering.

The angular scattering coefficient $\beta^{\lambda}(\theta)$ describes the amount of scattered light at a given wavelength λ in a given direction angle θ. It is given by,

$$\beta(\theta) = \frac{\pi^2 \left(n^2 - 1\right)^2}{2N\lambda^4} \left(\frac{6 + 3p_n}{6 - 7p_n} \right) \left(1 + \cos^2 \theta\right) \tag{2.1}$$

The total scattering coefficient β describes the total amount of light removed from a viewing path by scattering. It is given by,

$$\beta = \int_0^{4\pi} \beta(\theta) d\Omega = \frac{8\pi^3 (n^2 - 1)^2}{3N\lambda^4} \left(\frac{6 + 3p_n}{6 - 7p_n} \right) \tag{2.2}$$

where θ is the angle between the viewing path and the sun direction, n is the refractive index of air with the value of 1.0003 in the visible band, N is the number of molecules per unit volume (molecular density), with the value of 2.545×10^{25} for air at standard temperature and pressure p_n is the depolarization factor with the standard value of 0.0035 for air. Therefore, the total scattering coefficient for the blue light (400nm) is $2.44 \times 10^{-5} m^{-1}$, for the green light (530nm) is $1.18 \times 10^{-5} m^{-1}$ and for the red light (700nm) is $6.95 \times 10^{-6} m^{-1}$. This explains why the blue light is scattered more than the red light hence the dominant blue colour of the sky.

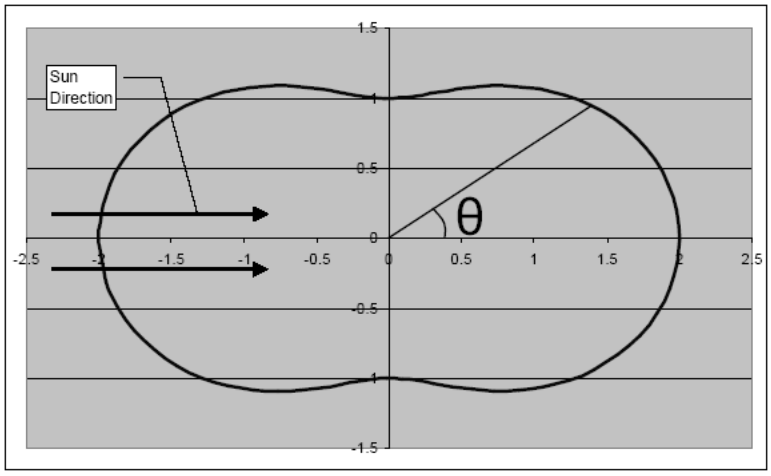

Figure 2.4 The shape of the Rayleigh phase function.

Angular scattering coefficient is equivalent to the total scattering coefficient multiplied with the phase function. The phase function for Rayleigh scattering $f_{air}(\theta)$ is given by,

$$f_{air}(\theta) = \frac{3}{16\pi} (1 + \cos^2 \theta) \tag{2.3}$$

2.2.2 Mie Scattering

Larger particles scatter strongly in the forward direction. This particular scattering phenomenon is termed as Mie scattering. The scattering is inversely proportional to the second order of the particle size and is independent of wavelength.

Mie scattering is applicable to scattering caused by particles of any size. Thus, Rayleigh scattering is actually a subset of Mie scattering. Notice that, Mie scattering theory will yield similar results as Rayleigh scattering when applied to small particles. In Figure 2.5, the top left image is identical to Rayleigh phase function, proving that Rayleigh scattering theory is actually a subset of Mie scattering for smaller particles ($r < \lambda/10$). Nevertheless, Mie scattering is commonly used exclusively for larger particles (aerosols).

The phase function for Mie scattering was approximated by Henyey-Greenstein (Henyey, 1941) and is given by the following equation,

$$f_{HG}(\theta) = \frac{1}{4\pi} \frac{1 - g^2}{\left(1 - 2g\cos\theta + g^2\right)^{3/2}} \tag{2.4}$$

Positive values of g represent forward scattering and negative values of g represent backward scattering.

The total scattering coefficient is given by,

$$\beta = 0.434 c \pi \left(\frac{2\pi}{\lambda}\right)^{v-2} K \tag{2.5}$$

where c is the concentration factor with its value varies around 6 x 10^{-17} to 25 x 10^{-17} as the turbidity increases, v is the Junge's exponent with a standard value of 4 for a sky model and K varies from 0.656 for 400nm to 0.69 for 770nm.

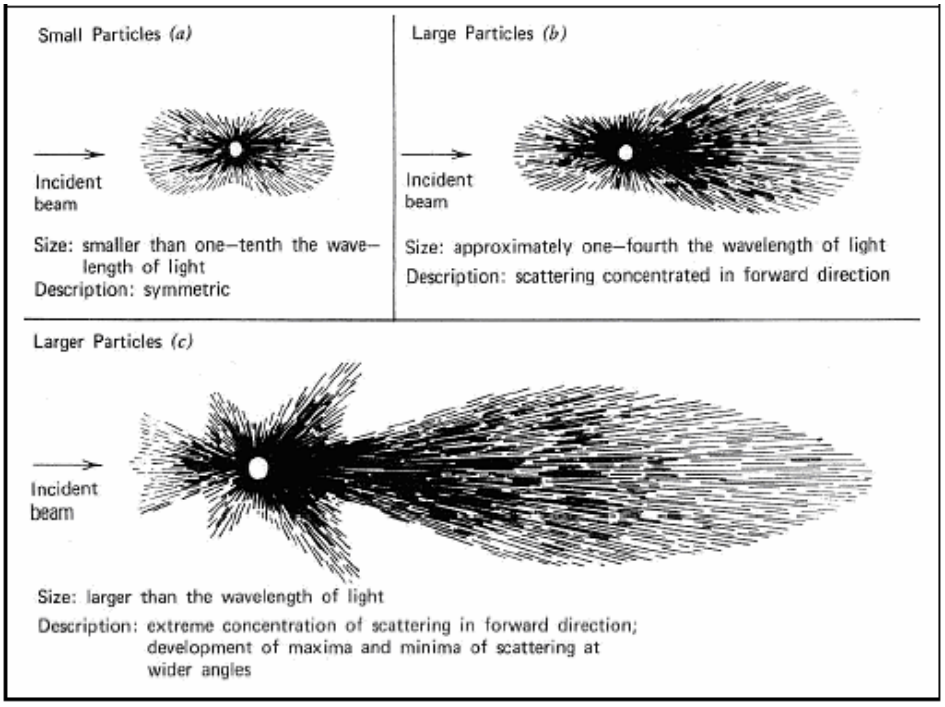

Figure 2.5 The shape of the Mie phase function.

2.2.3 Absorption

Absorption is a process when a particle converts a part of its incident energy with the incoming light into another form: photo-chemical processes, heating et cetera. Light is mostly absorbed by gases in the atmosphere such as oxygen, ozone and nitrogen dioxide.

Transmittances due to the gaseous absorption are usually modeled using Bouguer's Law. It is given by,

$$T_\lambda = \exp(-m\tau_\lambda) \tag{2.6}$$

where

$$\tau_\lambda = uA_\lambda \tag{2.7}$$

is the absorption optical thickness, m is the optical mass, u is the reduced path length (in atm-cm), and A_λ is the volume absorption coefficient. The volume absorption coefficient expresses the total losses caused by absorption per unit length along the viewing path.

2.2.4 Atmosphere Density

The Earth's atmosphere consists of four separate layers: i) troposphere (extends up to 12km), ii) stratosphere (extends up to 53km), iii) mesosphere and iv) thermosphere. The first two layers constitute 99% of the total atmosphere. Gravity holds the atmospheric contents to the Earth's surface, thus explaining the decreases in density with altitude (see Figure 2.6(a)).

The contents of the Earth's atmosphere are: i) various gases (NO_2 - 78%, O_2 - 21%, and others - 1%), ii) water vapour and ii) aerosols. Their density vary with altitude and depends on both solar heating and geomagnetic activity. The simplest approximation of the relationship between the atmospheric density and altitude would be an exponential fall-off model in which the density decreases exponentially with altitude.

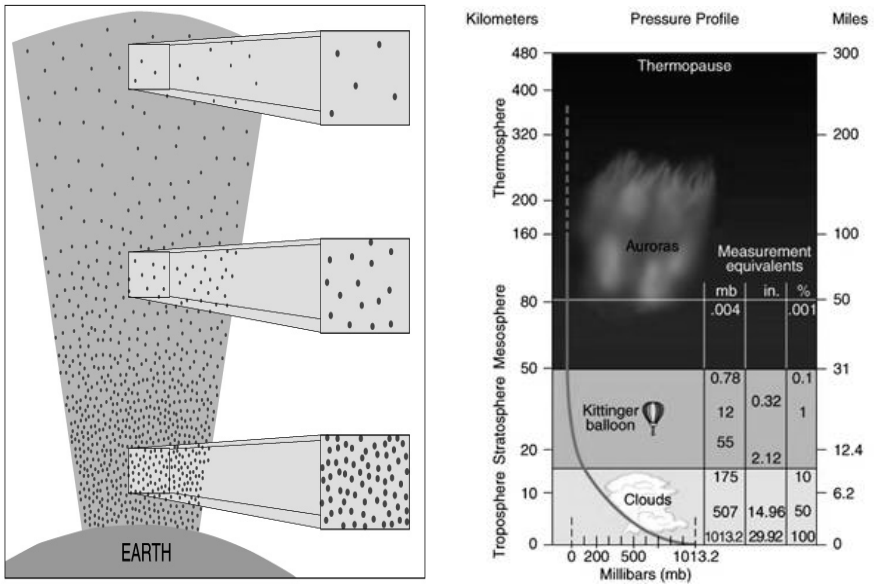

(a) (b)

Figure 2.6 Earth's atmosphere density.

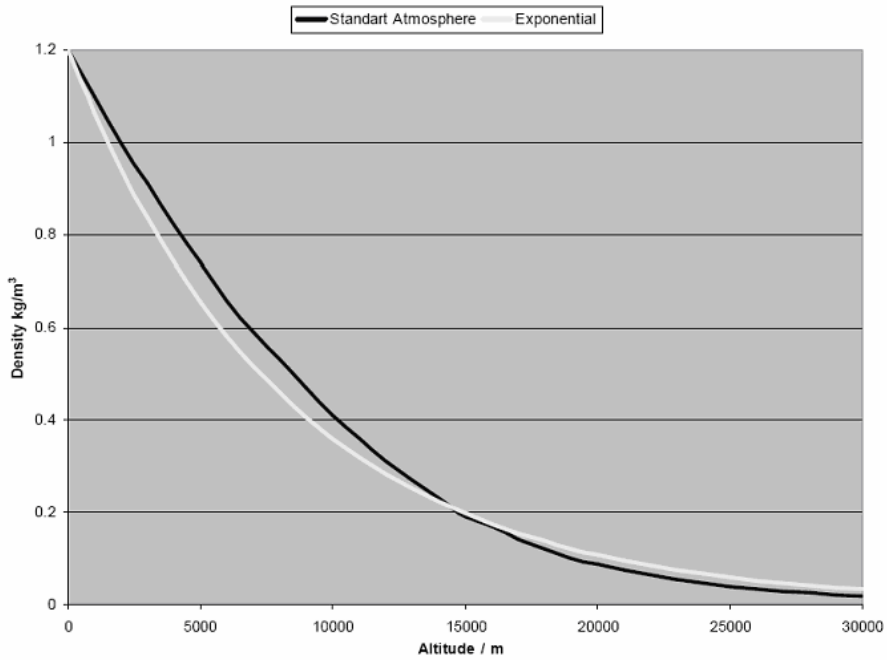

Figure 2.7 The density of the US Standard Atmosphere vs. the density approximated by a simple exponential model.

(McCartney, 1976) modeled the atmosphere by 7 layers up to 86km; each with its own individual pressure, temperature and density values. McCartney's

model was later adopted by COESA (Committee on Extension to the Standard Atmosphere) as the US Standard Atmosphere. McCartney's model is considered as a more accurate approximation of the Earth's atmospheric density profile than the simple exponential model, yet result between those two shows minimal disparity (see Figure 2.7).

2.2.5 Explanation on the Daylight Sky Colour Phenomenon

2.2.5.1 Variations of the Sky Colour Distribution over the Skydome

The daylight sky colour distribution can be described as an interchange between these three effects (Minnaert, 1954):

i. The sky intensity increases (becoming whiter) rapidly as it gets closer to the sun.
ii. The darkest blue colour on the entire sky dome is usually found at an area perpendicular (90°) to the sun.
iii. The sky intensity increases towards the horizon (the deep blue colour lessens and becomes whiter).

The first effect is caused by the Mie scattering. The strong directional dependency of the Mie scattering causes the sky intensity to increase rapidly as the view get closer to the sun. Meanwhile, the relatively weak dependency on wavelength causes the whitening of the sky area surrounding the sun.

The second effect, the low intensity of the sky colour at an area perpendicular to the sun is explained by the shape of the phase function for the Rayleigh scattering. At an angle of 90° from the sun, the scattering volume is roughly half of the scattering volume in the forward and backward direction (see Figure 2.4). In addition, larger Mie scatterers hardly scatter any light at such a large angle. As a result, a visible dark band is thus formed at that particular sky area (90° from the sun)

due to the appalling contrast with the neighbouring two opposing bright regions. In nature however, this effect is hardly visible and is only noticeable on a very clear day. Most of the time, the high contrast is evened out due to the multiple scattering effect minimizing the differences in intensity and also by the logarithmic mapping of intensities done by the human vision system.

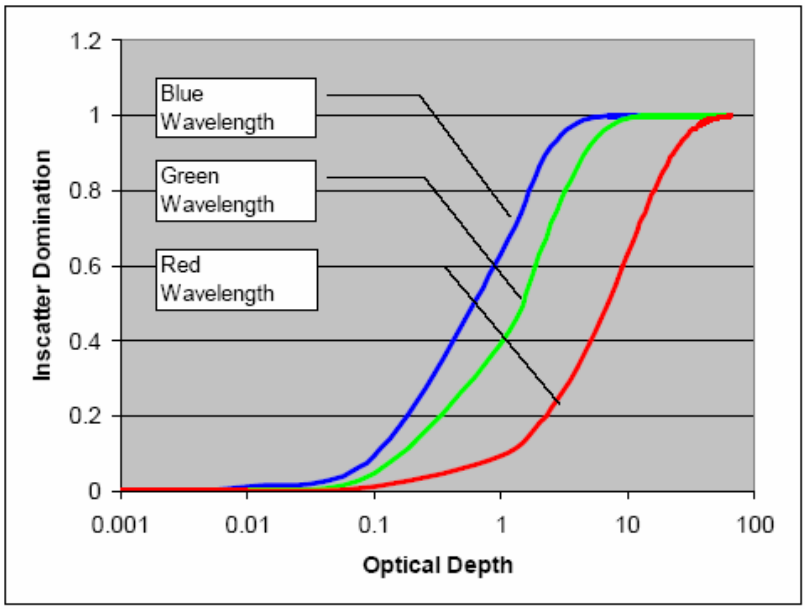

Figure 2.8 Optical depth vs. in scatter domination.

The third effect is the result of the increasing optical depth for the given viewing path. When the view direction approaches the horizon, the shape of the atmosphere causes the light to travel at a longer distance before finally reaching the observer eyes. Since the optical depth of a given viewing path close to the horizon is large enough to resemble infinity, the travelling light gets scattered and absorbed over and over again. This repetitive process increases the probability of the blue light to be attenuated from the viewing path. Although the in scattering coefficient of the blue light is approximately ten times that of the red light, the extinction is equally larger. As a result, the resulting spectral intensities is evened out for all of the visible wavelengths (see Figure 2.8); producing an almost whitish colour.

This raises the question of why the horizon becomes yellow, red or even orange during sunrise and sunset instead of white (the colour of the horizon during a higher sun altitude). The answer is because of the initial skylight (diffuse) colour. For high sun altitudes, the skylight has been travelling through a lesser volume of the Earth's atmosphere (optical depth) before entering the current viewing path. Hence the blue portion of the initial skylight is still largely intact. At a lower sun altitude (close to the horizon), the skylight has been travelling through a greater volume of the Earth's atmosphere (optical depth) before entering the current viewing path. The blue portion of the initial skylight has been largely diminished by then; leaving a yellowish, reddish or even oranges colour of the light.

The darkening of the sky area close to zenith whilst the horizon stays white and bright as the observer altitude increases is also explained by Figure 2.8 above. The optical depth of these viewing paths (close to zenith) gets significantly smaller as the observer increases his or her altitude. Consequently, the amount of blue light being attenuated is far smaller, resulting to a more intense blue colour at that particular area of the sky.

2.2.5.2 Visibility

The term visibility is widely used in the atmospheric optics field to represent the opaqueness level of a medium (atmosphere) of which the light has to travel through before reaching the observer's eyes. This value is determined by the amount of dust particles and moistures present in the atmosphere.

Variations in visibility are usually represented by the turbidity parameter. Turbidity is the measure of the fraction of scattering due to haze as opposed to molecules. This is a convenient quantity since it can be estimated based on the visibility/transparency of a distant object. More formally, turbidity is the ratio of the

optical thickness of a haze-filled atmosphere (haze particles and molecules) to the optical thickness of a pure molecular atmosphere:

$$T = \frac{t_m + t_a}{t_m} \tag{2.8}$$

where T is the turbidity, t_m is the vertical optical thickness of a pure molecular atmosphere and $t_m + t_a$ is the vertical optical thickness of a haze-filled atmosphere.

2.2.6 Explanation on the Aerial Perspective Effects Phenomenon

Aerial perspective effects can be divided into two types: i) the loss of contrast and ii) colour shifts. Both effects intensify with distance. These two effects act as the visual cue for indicating the scale and distance. The loss of contrast is comprehensible since this effect simply the result of the Beer's Law; the further the object from the camera, the more likely that it will take on the atmosphere's colour. However, the colour shifts effect requires a little bit more explanation.

Figure 2.9 shows an illustration of the colour shifts effect. There are two parallel-vertical planes, one black and one white, receding into infinity. Note how the black plane turns blue with distance while the white plane turns red.

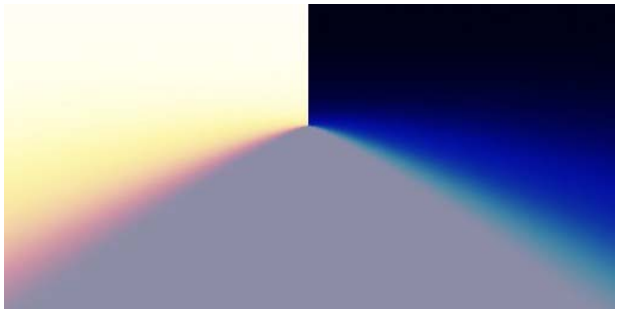

Figure 2.9 Aerial perspective colour shifts.

2.3 Rendering the Atmospheric Effects

2.3.1 Basic Problems

2.3.1.1 Sky Colour

To determine the spectral distribution of light (the sky colour) incident on the camera (the observer's eyes) positioned at P_v, an integral along the viewing path P_v – P_a is required.

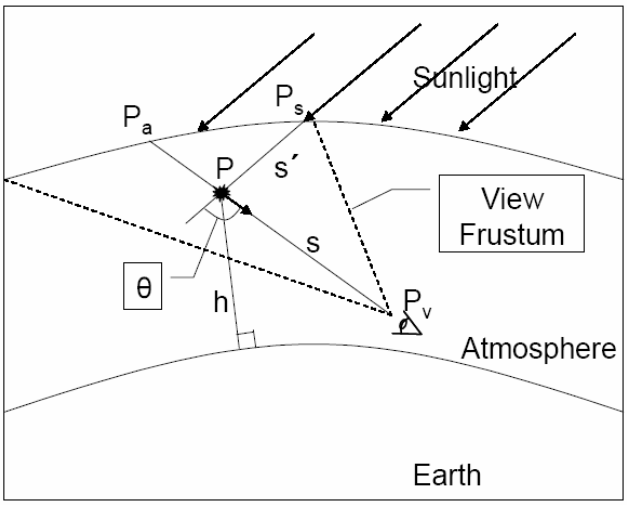

Figure 2.10 Single scattering of sunlight.

For each point *P* along the path, the single light scattering equation need to be evaluated, resulting in the following integral (Nishita et al, 1996),

$$I_v(\lambda) = \int_{P_v}^{P_a} I_{sun}(\lambda) \cdot F(\lambda, s, \theta) \cdot e^{\left(-t(s,\lambda) - t(s',\lambda)\right)} ds \qquad (2.9)$$

where $I_{sun}(\lambda)$ is the incident intensity of sunlight at the given wavelength on the atmosphere. $F(\lambda, s, \theta)$ is given by,

$$F(\lambda, s, \theta) = \beta_R(\lambda) \cdot \rho_R(s) \cdot \beta_R(\theta) \quad + \quad \beta_M(\lambda) \cdot \rho_M(s) \cdot \beta_M(\lambda, \theta) \qquad (2.10)$$

where $\beta_R(\lambda)$ and $\beta_M(\lambda)$ are the Rayleigh and Mie total scattering coefficients, ρ_R and ρ_M are the density of the Rayleigh and Mie scatterers. The value for the molecular density distribution can be accurately approximated using an exponential function given by,

$$\rho_R(h) = \rho_0 \cdot e^{-\frac{h}{8300m}} \qquad (2.11)$$

$\beta_R(\theta)$ and $\beta_M(\lambda, \theta)$ are the scattering phase functions for Rayleigh and Mie scattering respectively. The optical depth of path *s*, $-t(s, \lambda)$, and path *s'*, $-t(s', \lambda)$, can be written as,

$$t(s, \lambda) = \beta_R(\lambda) \int_0^s \rho_R(l) dl \quad + \quad \beta_M(\lambda) \int_0^s \rho_M(l) dl \qquad (2.12)$$

When substituting Equation (2.12) into (2.9), the result is a double nested integral.

Equation (2.9) is only valid when multiple scattering and back-scattering of light from the Earth are ignored. Adding a second order scattering requires solving equation (2.9) as an integral function over the total solid angle at every point *P* along the viewing path.

2.3.1.2 Aerial Perspective Effects

Similar to the sky colour, an integral along the viewing path $P_v - P_o$ is required to calculate the final colour of the distant object. In this case, the single scattering equation is given by,

$$I_v(\lambda) = I_o(\lambda) \cdot \int_{P_v}^{P_o} e^{-t(s,\lambda)} ds \quad + \quad \int_{P_v}^{P_o} I_{sun}(\lambda) \cdot F(\lambda, s, \theta) \cdot e^{\left(-t(s,\lambda) - t\left(s',\lambda\right)\right)} ds \tag{2.13}$$

The difference between Equation (2.13) and (2.9) is the radiance value of $I_o(\lambda)$. For the sky, $I_o(\lambda)$ is fixed to zero (black), leaving only the second integral to be solved. For a distant object, $I_o(\lambda)$ is allowed to take on any value. $I_o(\lambda)$ is the spectral distribution of light leaving P_o, which is a combination of sunlight, skylight and light reflected from the Earth. The resulting irradiance is then multiplied by the material's BRDF at P_o to give the exiting radiance value.

2.3.1.3 RGB-Colour from Spectral Distribution

By the time the light reaches the observer's eyes, its spectral information will be detected by antenna-like nerve endings (rods and cones) and send as signals to the brain to be processed. Human eyes are capable of detecting different intensities and colours of light. Both depend on the spectral distribution of the incoming visible radiation. Note that the human eyes are only sensitive to the region of 380nm – 780nm of the incoming electromagnetic spectrum (light).

If a computer display (monitor) is used to visualize the light, its spectral distribution must first be converted to a displayable colour space. CIE carried out a colour matching experiment in 1931, resulting to the introduction of the tristimulus XYZ-colour space. It has been the standard preference for researchers throughout the years for the basis of colorimetry calculation. The XYZ-colour space is based on

the principle that the human retina has three types of photoreceptor cone cell; each responding to the incident light with different spectral response curve (see Figure 2.11). Since there are exactly three photoreceptors in the human retina, only three values are needed to describe the colour of the incident light, hence the usage of the tristimulus concept. Colour vision according to (Poynton, 1995) is indeed inherently trichromatic.

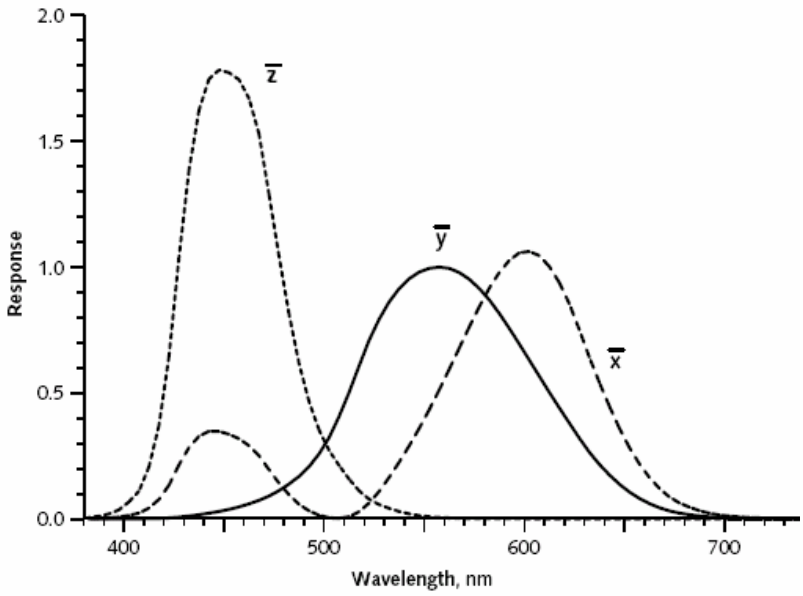

Figure 2.11 CIE's three colour matching functions, $\bar{x}$, $\bar{y}$ and $\bar{z}$.

The tristimulus values (XYZ) are computed by integrating the continuous spectral power distributions (SPDs); computed using the three colour matching functions obtained from the experiment. The three colour matching functions, $\bar{x}$, $\bar{y}$ and $\bar{z}$ were determined by measuring the mean colour perception of a sample of human observers over the visual range of 380nm – 780nm.

The 1931 experiment produced a colour matching function set, the "*2º Standard Observer*", intended for a 2º field-of-view purpose. In 1964, CIE added another set of the colour matching function based on the 10º field-of-view and is referred as the "*10° Supplementary Standard Observer*". Each Observer has its own separate set of colour matching function. The CIE colour matching function gives

the relative contributions of light with wavelength λ to the XYZ tristimulus value. The XYZ tristimulus value can then be calculated by integrating the multiplication result of the reflectance values *R(λ)*, the relative spectral energy distributions of the CIE Illuminant *S(λ)*, and the Standard Observer colour matching functions *x(λ)*, *y(λ)*, and *z(λ)*. The integration is approximated by the following summation,

$$X = \int_{380}^{780} S(\lambda)x(\lambda)R(\lambda)$$
$$Y = \int_{380}^{780} S(\lambda)y(\lambda)R(\lambda) \qquad (2.14)$$
$$Z = \int_{380}^{780} S(\lambda)z(\lambda)R(\lambda)$$

The XYZ-colour space acts as the intermediary between the spectral distribution and a host of device-dependent colour spaces. For a typical computer display purpose, XYZ is usually converted to RGB using a 3x3 matrix transform. Generally, a predefined matrix set is chosen unless the monitor specific phosphor chromaticities are known. Nevertheless, this conversion leads to a significant predicament. Converted values may lies outside the RGB gamut thus producing an impossible colour to display in a standard CRT monitor. A variety of schemes can be used to map the unrepresentable colour into a device's gamut. A simple approach, implemented in this research, which often yields acceptable results, is by reducing the saturation of the requested colour until it falls within the possible RGB gamut. Additional tone mapping techniques to solve this problem can be found in (Ferwerda, 1996; Larson, 1997 and Tumblin, 1993).

2.4 Previous Works

2.4.1 Simulation-Based Methods

(Klassen, 1987) was the first person to propose a solution to the basic light scattering problem. The atmosphere is modelled as two layers (see Figure 2.12), with the top layer treated as a pure molecular layer and the bottom layer as a mixture of molecules and aerosols. By assuming each layer density as constant, the problem is hugely simplified since it allows a minimal calculation of the optical depth. To determine the correct optical depth of each layer, Klassen uses geometric computations that account for the curvature of the atmosphere. The scattering problem is now reduced to integrating an analytical equation along the path for each layer.

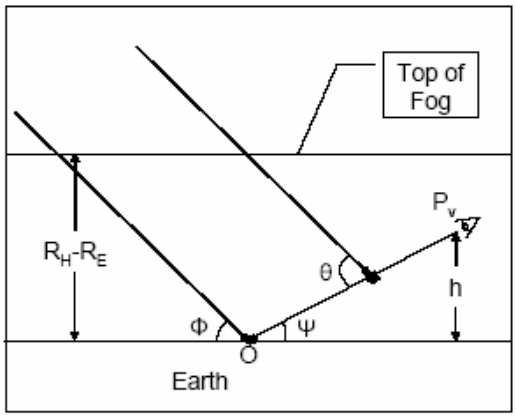

Figure 2.12 Klassen's model of the fog layer.

(Kaneda et al, 1991) employed a similar concept to Klassen but instead of modelling the atmosphere as a two-layer structure (two values of optical depth only), they modelled it as a spherical shape dome with an exponential decay density distribution.

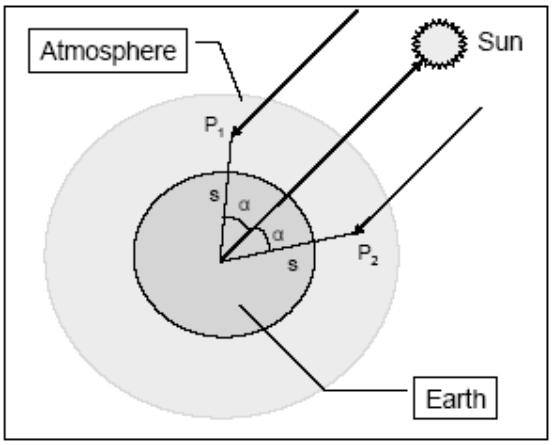

Figure 2.13 Nishita et al's cylindrical coordinates system.

(Nishita et al, 1996) proposed a method based on the exponential distribution of molecules and aerosols in the atmosphere. Their method takes into account the second order of scattering. This is done by precalculating the intensity distribution at a large number of voxels. The irradiances for a number of directions (buckets) are then stored in a look-up table. These stored intensities are then referred to when gathering the second order reflected light for a single scattering event. Since the above calculation will involve a heavy computational load, (Nishita et al, 1996) developed a cylindrical coordinates system (see Figure 2.13) to speed up the calculation. The atmospheric length is axis-symmetric, meaning that the points that share the same α and distance s will also share the same optical depth from the sun.

2.4.2 Analytical-Based Methods

Analytical-based methods were developed for the purpose of offline image synthesis. These methods are parametric in nature and were based on the fits of simulated or measured data. Amongst the earliest analytical models introduced were (Kittler CIE, 1994) and (Moon and Spencer CIE, 1994). (Kittler, 1994) clear sky luminance formula is given by,

$$Y_z \frac{\left(0.91+10e^{-3\gamma}+0.45\cos^2\gamma\right)\left(1-e^{-0.32/\cos\theta}\right)}{\left(0.91+10e^{-3\theta s}+0.45\cos^2\theta s\right)\left(1-e^{-0.32}\right)} \tag{2.15}$$

where Y_z is the zenith luminance. The zenith luminance can either be calculated using an existing analytical model or from a measured data source. (Moon and Spencer CIE, 1994) developed a formula for calculating the luminance distribution of an overcast sky,

$$Y_z\left(1+2\cos\theta\right)/3 \tag{2.16}$$

Perez et al (1993) developed a five-parameter model to describe the all-sky luminance distribution. Each parameter has a specific physical effect on the sky colour distribution. The parameters are (a) darkening or brightening of the horizon, (b) luminance gradient near the horizon, (c) relative intensity of the circumsolar region, (d) circumsolar region width and (e) relative backscattered light. These basis functions can be fit to any data; the five parameters are able to capture the overall characteristics of the daylight sky distributions without ringing or data explosion. Perez et al's (1993) model is given by,

$$F\left(\theta,\gamma\right)=\left(1+Ae^{B/\cos\theta}\right)\left(1+Ce^{D\gamma+E\cos^2\gamma}\right) \tag{2.17}$$

where A, B, C, D and E are the distribution parameters. The luminance, *Y*, for the sky in any viewing direction depends on the distribution function and the zenith luminance. It is given by,

$$Y=Y_z\,F\left(\theta,\gamma\right)/F\left(0,\theta_s\right) \tag{2.18}$$

Perez et al's (1993) model is quite similar to the CIE models, but has been found to be slightly more accurate if the five distribution parameters are chosen wisely (Ineichen, 1994).

(Preetham et al, 1999) used (Nishita et al's, 1996) method to calculate the skylight. To simplify the calculation, they ignored both ground reflection, third and higher order scattering. The sunlight was calculated using (Iqbal's, 1983) method. The calculation was repeated for a variety of turbidity and sun position; at 343 directions (endpoint) on the sky dome. The data obtained is subsequently fitted using (Perez et al's, 1993) luminance formulation (see Equation 2.18). The fitting process was done for luminance Y, chromaticity x and chromaticity y. The coefficients for the Yxy distribution functions are given by,

$$\begin{bmatrix} A_Y \\ B_Y \\ C_Y \\ D_Y \\ E_Y \end{bmatrix} = \begin{bmatrix} 0.1787 & -1.4630 \\ -0.3554 & 0.4275 \\ -0.0227 & 5.3251 \\ 0.1206 & -2.5771 \\ -0.0670 & 0.3703 \end{bmatrix} \begin{bmatrix} T \\ 1 \end{bmatrix} \tag{2.19}$$

$$\begin{bmatrix} A_x \\ B_x \\ C_x \\ D_x \\ E_x \end{bmatrix} = \begin{bmatrix} 0.0193 & -0.2592 \\ -0.0665 & 0.0008 \\ -0.0004 & 0.2125 \\ 0.0641 & -0.8989 \\ -0.0033 & 0.0452 \end{bmatrix} \begin{bmatrix} T \\ 1 \end{bmatrix} \tag{2.20}$$

$$\begin{bmatrix} A_y \\ B_y \\ C_y \\ D_y \\ E_y \end{bmatrix} = \begin{bmatrix} -0.0167 & -0.2608 \\ -0.0950 & 0.0092 \\ -0.0079 & 0.2102 \\ 0.0441 & -1.6537 \\ -0.0109 & 0.0529 \end{bmatrix} \begin{bmatrix} T \\ 1 \end{bmatrix} \tag{2.21}$$

By using the Perez et al's (1993) formulation (see Equation 2.18), all three components of Yxy can be calculated based on the distribution functions given above. Chromaticities x and y are similarly behaved thus given by the same model as luminance Y (Preetham et al, 1999),

$$x = x_z \frac{F(\theta, \gamma)}{F(0, \theta_s)} \tag{2.22}$$

$$y = y_z \frac{F(\theta, \gamma)}{F(0, \theta_s)} \tag{2.23}$$

2.4.3 Aerial Perspective-Based Methods

Aerial perspective-based methods employed a single rendering equation, implemented as a pixel/vertex-based shader, for both sky and distant objects. The differences between those two were their initial colour and distance (optical depth) from the camera. The sky initial colour is black whilst for the distant objects; each has its own respective initial colour. The obvious advantage is the ability to simulate the atmospheric effects on both sky and distant objects using a single pixel/vertex-based equation. This nicely complements the modern graphic hardware rendering pipeline.

Hoffman and Preetham's method (2002) is based on a simplification of the atmospheric scattering theory. Their method is capable of compensating for many of the shortcomings suffered by the traditional range based fog. Unlike the traditional range based fog, both directional-dependency and wavelength-dependency of light are well captured. All pixels and vertices in the scene are evaluated using a single aerial perspective formulation,

$$L(s, \theta) = L_0 F_{ex}(s) + L_{in}(s, \theta) \tag{2.24}$$

According to (Hoffman and Preetham, 2002), the extinction coefficient and the in scattering component of a given viewing path are given by,

$$F_{ex}(s) = e^{-(\beta R + \beta M)s} \tag{2.25}$$

$$L_{in}(s,\theta) = \frac{\beta_R(\theta) + \beta_M(\theta)}{\beta_R + \beta_M} E_{sun}(1 - F_{ex}(s)) \tag{2.26}$$

where E_{sun} is the RGB-colour of the sunlight, β_R is the Rayleigh total scattering constant and β_M is the Mie total scattering constant. The two total scattering constants are given by,

$$\beta_R(\theta) = \frac{3}{16\pi} \beta_R(1 + \cos^2\theta) \tag{2.27}$$

$$\beta_M(\theta) = \frac{1}{4\pi} \beta_M \frac{1 - g^2}{(1 + g^2 - 2g\cos\theta)^{3/2}} \tag{2.28}$$

(Hoffman and Preetham's, 2002) method suffered from several visual artefacts, as reported in (Nielsen, 2003). The direct uses of simplified theoretical models for the task of mapping the intensities to the RGB-colour space had causes the visible dark band effect to appear at the sky area perpendicular to the sun (Nielsen, 2003). This is visually wrong since the dark band effect is usually minimized by the multiple scattering of light, and by the logarithmic mapping of intensities to display the colour values done by the human vision system. Besides that, the Hoffman and Preetham's method treats the optical depth as a distance between the two endpoints (camera –object) to simplify the problem; by assuming the Earth's atmosphere density as constant in the process.

(Nielsen, 2003) improvised the (Hoffman and Preetham's, 2002) method to consider the atmospheric density changes between the Earth's atmosphere layers. He also corrected some of the visual flaws inherited from the original (Hoffman and Preetham's, 2002) model, albeit using less than accurate solving methods.

To lessen the visible dark band effect, (Nielsen, 2003) introduced a reducing factor $(1/2)$ to the $\cos^2(theta)$ part of the Rayleigh scattering phase function (see Equation 2.27). This solution is far from physically correct, but it does provide a reasonably good result. (Nielsen's, 2003) modified Rayleigh scattering phase function is given by,

$$\beta_R(\theta) = \frac{3}{16\pi}\beta_R\left(1+\frac{1}{2}\cos^2\theta\right) \tag{2.29}$$

Nielsen's aerial perspective formulation is based on the (Hoffman and Preetham's, 2002) model (see Equation 2.24). To expand the original method to consider a non-constant density atmosphere, the depth parameter is modified to consider both the observer's altitude and the object's altitude. The new $F_{ex}(s)$ formulation is given by,

$$F_{ex}(s) = e^{-(\beta R \cdot sR + \beta M \cdot sM)} \tag{2.30}$$

where s_R and s_M are the Rayleigh and Mie scattering optical depth of the given viewing path respectively. Nielsen (2003) also introduced a series of simple functions to determine the Rayleigh and Mie scattering optical depths for each frame, based on the current observer's altitude. Once more, these functions are far from physically correct, yet they manage to capture the darkening effect of the sky area close to the zenith at high observer's altitude correctly.

Table 2.1 A comparison made between the three groupings of previous methods, in term of a flight simulator domain's requirements.

Requirement	Group		
	Simulation-based	**Analytical-based**	**Aerial-perspective-based**
	Yes or no, please elaborate		
Able to simulate all possible daylight skies	Yes	Yes	Yes
Able to simulate the aerial perspective effects	No	Yes, but only for an offline image synthesis	Yes
Consider the scattering of light?	Yes, but only up to the second order of scattering	Yes, support multiple scattering	Yes, but only up to the second order of scattering
Consider the absorption of light?	No	Yes	No
Support a real-time arbitrary-moving camera?	Yes	No	Yes
Capture the darkening effect of the sky area close to zenith as the observer's altitude increases?	No	No, since the sky colour distribution data was captured at ground-level only	Only some of the methods are capable in doing so

CHAPTER 3

METHODOLOGY

3.1 Introduction

This chapter describes the methodology of this research. The methodology is explained using a *top-down* approach for easier understanding. Hence, the run-time processing module is described first, followed by the pre-processing module.

The research methodology is consisted of six steps. These steps are further grouped into two separate modules (see Figure 3.1): i) pre-processing module and ii) run-time processing module. These modules are designed to be implemented modularly.

As the name implied, the pre-processing module is performed first and only once. The purpose of this module was to prepare a look-up table that will be use during the run-time processing module. The four steps involved in this module are almost identical to the simulation phase of Preetham et al's (1999) similar work. However, the differences lie at: i) the choice of the simulated data source and ii) unlike Preetham et al's (1999) simulation phase, the production of the sky distribution maps are not limited to the ones observed from the ground level (0km) only.

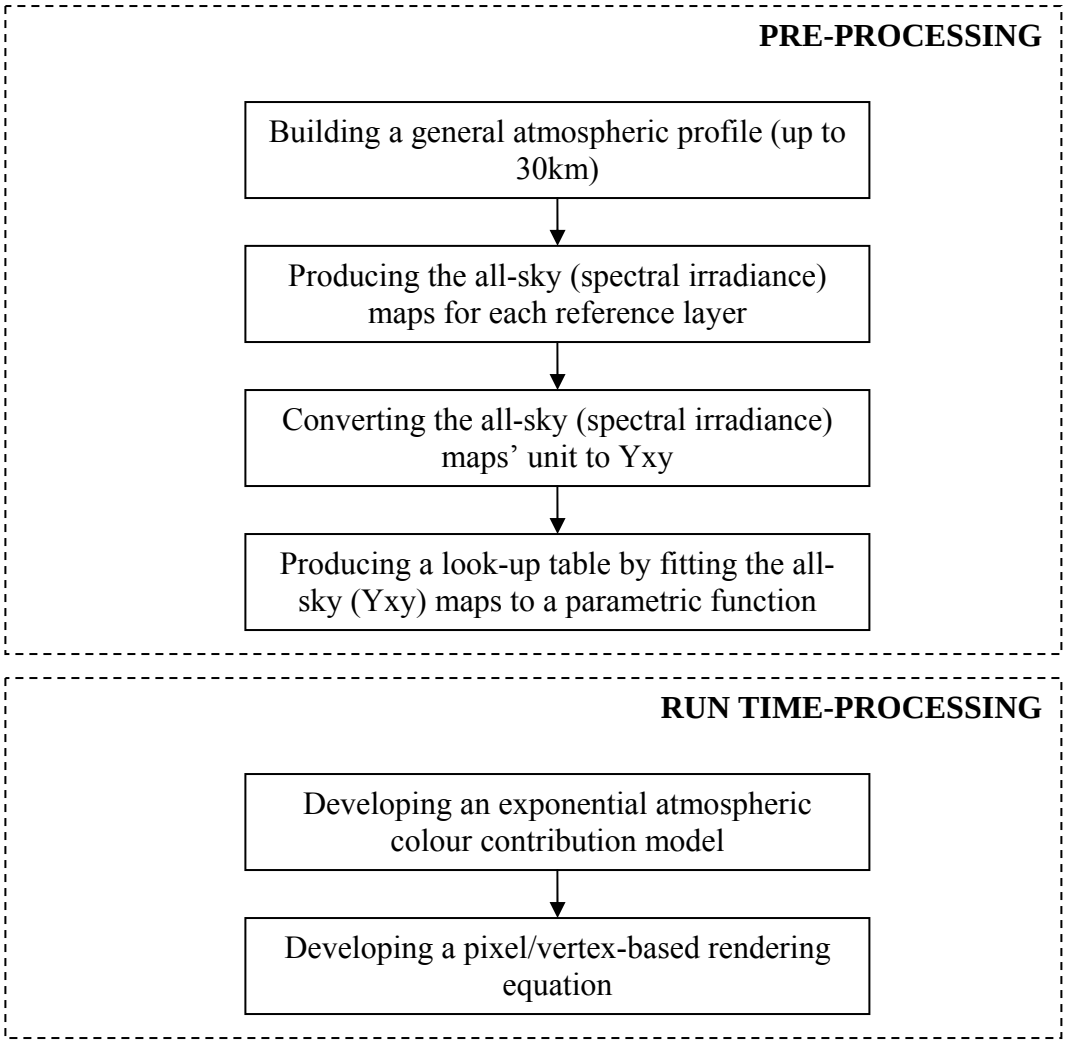

Figure 3.1 The research methodology.

The two steps involved in the run-time processing module were merged to produce the real-time rendering engine. The real-time rendering engine is executed each time the system receives updates to: i) the camera orientation/position, ii) the turbidity or iii) the sun position.

3.2 Run-Time Processing Module

3.2.1 Developing a Pixel/Vertex-Based Rendering Equation

This section describes the development of a single pixel/vertex-based rendering equation. The proposed equation took on the same form as the Beer's Law. It is given by,

$$RGB_{pv} = \sigma RGB_{obj} + (1-\sigma) RGB_{atm} \tag{3.1}$$

where RGB_{pv} represents the pixel/vertex's final colour, RGb_{obj} represents the object's initial colour, RGB_{atm} represents the atmosphere's colour contribution and σ is the viewing path's transparency. Note that the Beer's Law is not a physical model; there is neither provision for shadows/crepuscular rays (i.e., beams of light) in the atmosphere nor attempt to balance the energy transfer. Furthermore, RGB_{atm} in the original Beer's Law is simply is a fixed preset colour of the fog (usually white or grey). It does, however, simulate nicely the decrease in contrast with distance that characterizes real fog, smoke, and haze.

3.2.1.1 Transparency Calculation

The original Beer's Law does not take into account the non-uniform density of the Earth's atmosphere in its transparency calculation. The extinction coefficient ε is assumed to take on the same value regardless of the altitude (Considine, 1976). Therefore, the resulting optical depth τ is valid for the case of a single density medium only. Since the extinction coefficient ε actually varies with the altitude, the average value of ε over the viewing path is required for calculating its optical depth. Musgrave (1993) solved this problem by integrating ε over the vertical intervals traversed in the

viewing path. The resulting value is then normalized by the width of the interval. Musgrave's (1993) transparency model is given by,

$$\sigma(\varepsilon,\delta) = e^{-\varepsilon\delta} = e^{-\tau} \tag{3.2}$$

Optical depth τ is calculated by,

$$\tau = \frac{1}{z_2 - z_1}\left(-e^{-z1} - e^{-z2}\right) \tag{3.3}$$

where z_1 and z_2 are the altitude values of each endpoint for the given viewing path (observer – object). Equation (3.3) captures nicely the exponential relationship between the optical depth and the altitude. However, if the difference between z_1 and z_2 is too small to warrant a *division-by-zero* problem, the transparency is calculated using Equation (3.2) instead with ε replaced by,

$$\varepsilon = e^{-z1} \tag{3.4}$$

To translate the actual world's altitude (in km) to its equivalent virtual world value (coordinate *y*), the proposed model used a scale of 1:1.

3.2.1.2 RGB_{obj} and RGB_{atm}

RGB_{obj} is the initial RGB-colour of the object, with a fixed value of (0, 0, 0) for the background sky. RGB_{atm} is the RGB-colour contributed by the atmosphere to the viewing path.

RGB_{atm} is roughly equivalent to the $\int_{P_v}^{P_o} I_{sun}(\lambda) \cdot F(\lambda, s, \theta)$ part of the single scattering equation (see Equation 2.13) described in Chapter 2. Previous real-time aerial-perspective methods calculate the RGB_{atm} component on the fly, meaning that the component is re-calculated each time the system is updated. Unlike a sky model, aerial perspective effects cannot be stored in a simple function or precomputed table because they vary with distance and orientation (Preetham et al, 1999). This is the reason why the calculation has to be done in real-time at the first place.

This research explored the possibility of using an analytical-based approach to replace the real-time calculation of RGB_{atm}. The benefit is obvious; the ability to include physically accurate in scattering and extinction models. This can be accomplished without sacrificing the interactive frame rate performance; a near to impossible feat for the traditional real-time methods to achieve with the current hardware capabilities. Nevertheless, the implementation of the analytical-based approach should not interfere with the original reason why the RGB_{atm} component is calculated in real-time at the first place. The justifications and the development of the RGB_{atm} model are discussed next.

3.2.2 Developing an Exponential Atmospheric Colour Contribution Model

3.2.2.1 Justifications behind the Analytical vs. Real-Time Approach

Unlike the sky dome colour, aerial perspective effects cannot be precomputed for a given rendering. At every point on the viewing path, the single scattering equation must be solved. The resulting integral is a complex calculation that must be evaluated numerically.

Preetham et al (1999) advised that these two variables: i) distance and ii) orientation must be retained for the aerial perspective calculation. The rest of this section will prove that the developed model fulfils both obligations adequately.

Distance is taken into consideration in the aerial perspective component of the proposed model as a function of transparency. Transparency is the measure of opaqueness of the distant object. An object positioned far away from the observer will have a transparency value of nearly zero and vice versa. Thus, the proposed model is able to capture the different percentage of contrast loss and colour shifts of objects positioned in random distance from the observer.

Orientation is taken into consideration in the aerial perspective component of the proposed model as a function of RGB_{atm}. Rayleigh and Mie phase functions are dependent on the angular angle of the viewing path to the sun. Instead of using a fixed value, the RGB_{atm} may takes on different values based on the current sun position and the orientation of the camera (facing which endpoint on the sky dome). Thus, the proposed model is able to capture the directional-dependency of the scattering of light. For example, an object near to the sun will appears much brighter than a far object since the atmosphere-contributed colour of the viewing path (current endpoint) is of a higher intensity.

In conclusion, the proposed model managed to retain both variables: distance and orientation successfully in the aerial perspective effects calculation.

3.2.2.2 Exponential RGB_{atm} model

Before delving much further into the discussion, it is better to understand first the basic ideas behind the proposed exponential RGB_{atm} model. This model assumed that RGB_{atm} is the colour of the sky dome's endpoint currently being intersected by or

associated with the given viewing path. According to Musgrave (1993), the transparency $\sigma : 1 \to 0$ as distance, $\delta : 0 \to \infty$ (the opacity along the viewing path is 1-σ). Since the sky dome endpoints have an almost infinite distance from the observer (unobstructed viewing path), the transparency is therefore assumed as zero. As the result, the pixel/vertex-based shader takes on the full value of the RGB_{atm} colour. Meanwhile, if an object obstructs the sight at any point on the viewing path, the distance is therefore truncated, resulting to a transparency value of $\neq 0.0$. As the result, the pixel/vertex-based shader takes on a combination value of RGB_{atm} and RGB_{obj} colour.

There are three possible scenarios here: i) unobstructed viewing path truncated by the sky dome; ii) obstructed viewing path with the *projected path* truncated by the sky dome; and iii) obstructed viewing path with the *projected path* truncated by the Earth's surface. See Figure 3.2 (a) – (c) for an example of each scenario.

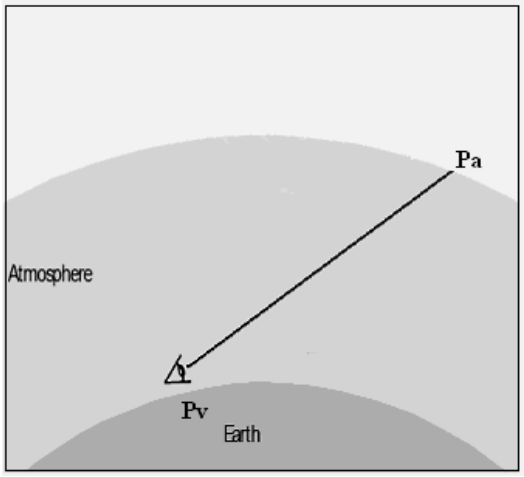

(a)

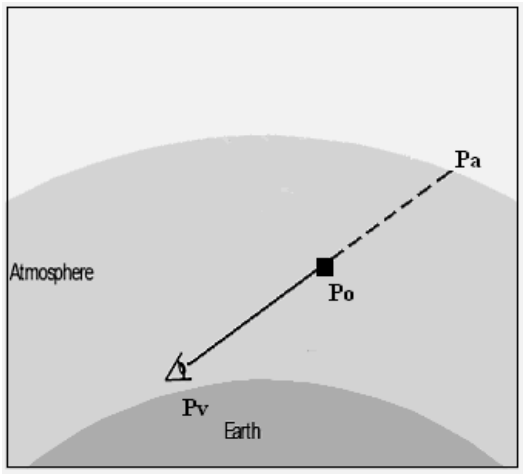

(b)

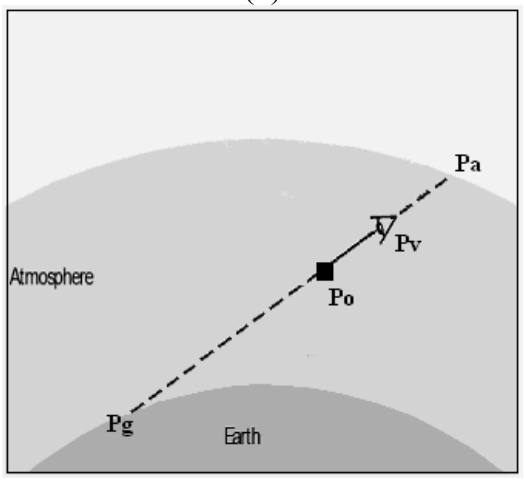

(c)

Figure 3.2 a) Scenario (i), b) scenario (ii) and c) scenario (iii).

Scenario (i) is the easiest scenario by far. Since the transparency value is equal to zero, the pixel/vertex-based shader will takes on the full RGB value of $\left(1-\left(0\right)\right)RGB_{atm}$.

Scenario (ii) is the second easiest scenario. The atmospheric contribution $\left(1-\sigma\right)RGB_{atm}$ at P_o is determined by multiplying the opacity with the RGB-colour of the sky dome's endpoint currently being intersected by or associated with the projected path at P_a (see Figure 3.2 (b)). This method is valid since the transparency value at each point P along the extended viewing path $P_v - P_o - P_a$, is integrated linearly to obtain the

final accumulated value at P_o. Therefore, the pixel/vertex-based shader will takes on a combination of $(1-\sigma)RGB_{atm}$ and $(\sigma)\,RGB_{obj}$ colour.

Scenario (iii) poses a relatively harder problem to solve compared to the earlier two scenarios. Scenario (iii) requires two parts of the *total* viewing path to be removed, $P_g - P_o$ and $P_v - P_a$. Therefore, the linear integral of transparency value is restricted to $P_v - P_o$. The atmospheric contribution $(1-\sigma)RGB_{atm}$ at P_o is determined by multiplying the accumulated transparency for $P_v - P_o$ with the RGB-colour of the current sky dome's endpoint currently being intersected by or associated with the viewing path at P_a (see Figure 3.2 (c)). The third scenario shares the same justification with the second scenario above.

So far, the scenarios of each possible viewing path composition have been explained in detail. However, before the RGB_{atm} component can be used in Equation (3.1), its own value must first be calculated. The value is obtained from the current sky distribution map; calculated each time the system is updated.

Since both atmosphere density and optical depth interpolate exponentially with the altitude, the colour of the viewing path (the sky dome's endpoint) must therefore be exhibiting the same behaviour. This logical assumption forms the basis of the proposed exponential RGB_{atm} model. To obtain a sky dome's endpoint colour at a particular altitude, the solution is to simply interpolate the value from the five similar endpoints at each reference layers' sky distribution map. So, each time the turbidity or the sun position parameter changes, the sky colour map for each reference layer will be updated accordingly.

These maps are prepared using the Perez et al's (1993) parametric function; calculated at each endpoint on the sky distribution map. The five parameters values, *ABCDE* are obtained from the look-table prepared earlier in Chapter 3.

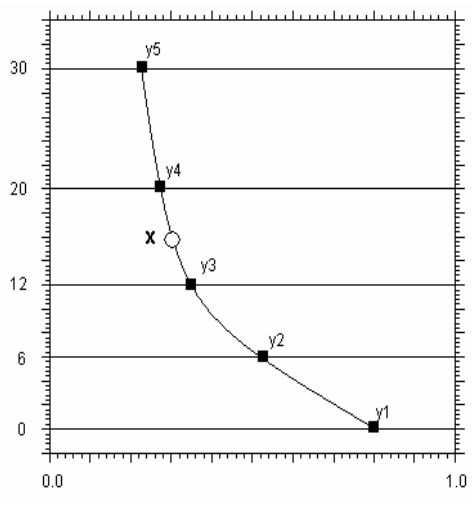

Figure 3.3 An example of the exponential interpolation scheme at work.

Figure 3.3 above provides an example of the exponential atmospheric colour contribution model at work. Using the 4-points Lagrange interpolation scheme, the selected endpoint's RGB-colour value at altitude *x* is obtained by interpolating the values of similar endpoints at all five reference layers y_1-y_5.

The last obstacle was to find a solution for finding the correct endpoint currently being intersected by or associated with the current viewing path. Generating the equation of line passing through these two points: i) the camera, P_0, and ii) the viewing path's endpoint, P_1 solves this problem. To find the equation of a line, these values are needed: i) a point on the line and ii) a vector having the direction of the line. The vector is determined by P_0 and P_1, $\overline{P_0P_1}$.

$$\overline{P_0P_1} = (x1 - x0)I + (y1 - y0)J + (z1 - z0)K \tag{3.5}$$

The line equation is thus given by,

$$x = x_0 + (x_1 - x_0)t \qquad y = y_0 + (y_1 - y_0)t \qquad z = z_0 + (z_1 - z_0)t \tag{3.6}$$

A test is then carried out for each stored sky dome endpoint's global coordinates. The endpoint's global coordinates that fulfil the line equation requirement is thus declared as the current RGB_{atm}. By stating an acceptable error-boundary value, the viewing path that did not intersect with any endpoints on the sky dome will be associated with the nearest one available.

3.3 Pre-Processing Module

There are two phases involved in the pre-processing module: i) simulation and ii) statistical fitting. The first three steps belong to the simulation phase whilst the fourth step belongs to the statistical fitting phase. These steps are described next in an ascending order.

3.3.1 Building a General Atmospheric Profile (Up to 30km)

This section describes the task of building a general atmospheric profile (vertical profile + effective path length) for altitudes up to 30km. Possible flight altitudes in a flight simulator should be within the range of 0km to 30km. This range value is required since the highest *sustained horizontal* flight altitude ever recorded is 85068 feet, approximately 26km (Miller, 1982).

The term "*general atmosphere*" is employed here since the atmospheric data used is not from a unique site. At present, no complete SMARTS2-compatible atmospheric profile up to 30km is available for free neither from the Internet nor from any published publications. This reason alone justified the decision to build a completely new atmospheric profile. The atmospheric profile is built from a

combination of actual measurements taken from various sites and by using mathematical formulas readily available from the scientific literatures.

Although the physical veracity of this profile are not guaranteed, it is sufficient for the purpose of rendering the daylight skies in a flight simulator system. What matter most is that the sky distribution characteristics such as the reddening of the sky horizon during sunset, the increase in yellow hue at sky area approaching the sun et cetera are eloquently captured. The simulated daylight skies should only need to convince the pilot that he or she is flying the plane during, for example, sunset, sunrise or mid-noon time setting and clear or overcast sky condition. The exact atmospheric profile for a specific location on Earth is thus deemed as unnecessary. Hence, the need for the pilot to differentiate between, for example, sunset sky in Paris and in Bangkok is deemed as irrelevant.

SMARTS2 model is chosen as the simulated data source primarily due to i) its parametric form and ii) its temperature/pressure-dependent extinction coefficients. Preetham et al's (1999) model employed Iqbal's (1983) method to calculate sunlight and Nishita et al's (1996) method to calculate skylight; combining both to produce the all-type of sky luminance distribution maps. Nevertheless, both methods assumed the density of the Earth's atmosphere as constant. Consequently, only skies observed at ground level (0km) could be simulated.

By providing either temperature or pressure value with respect to altitude, SMARTS2's extinction coefficients at exact atmospheric height (within the minimum and maximum altitude) can be interpolated. However, interpolation of the extinction coefficients in SMARTS2 is only allowed within the 0km-4km range. The provided atmospheric profile in SMARTS2 is only up to 4km, hence the range limitation. The rest of this section describes the task of building a completely new atmospheric profile up to 30km to represent the Earth's general atmosphere.

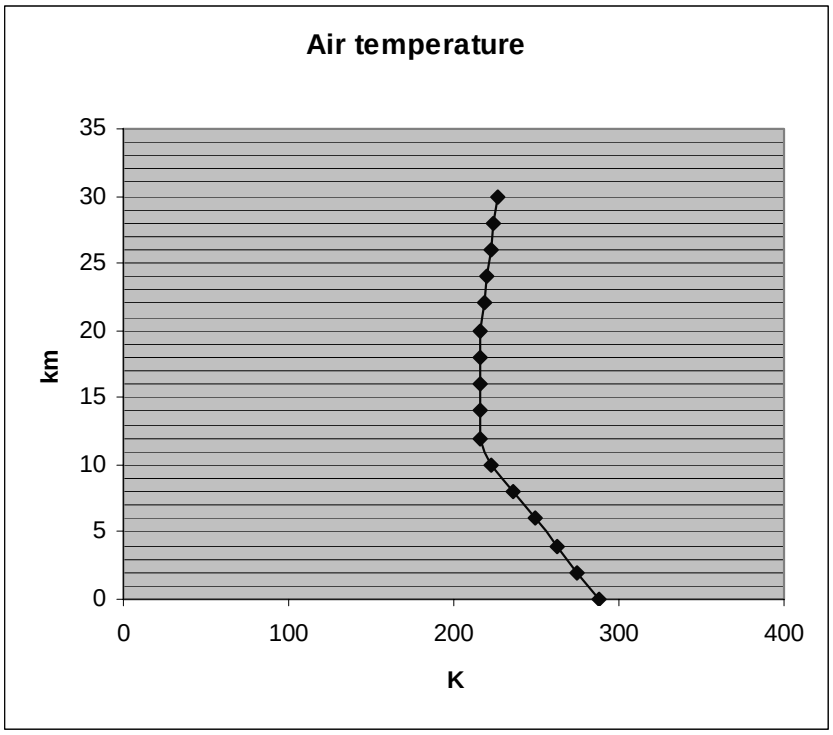
Air temperature
35
30
25
20
15
10
5
0
km
0
100
200
300
400
K

(a)

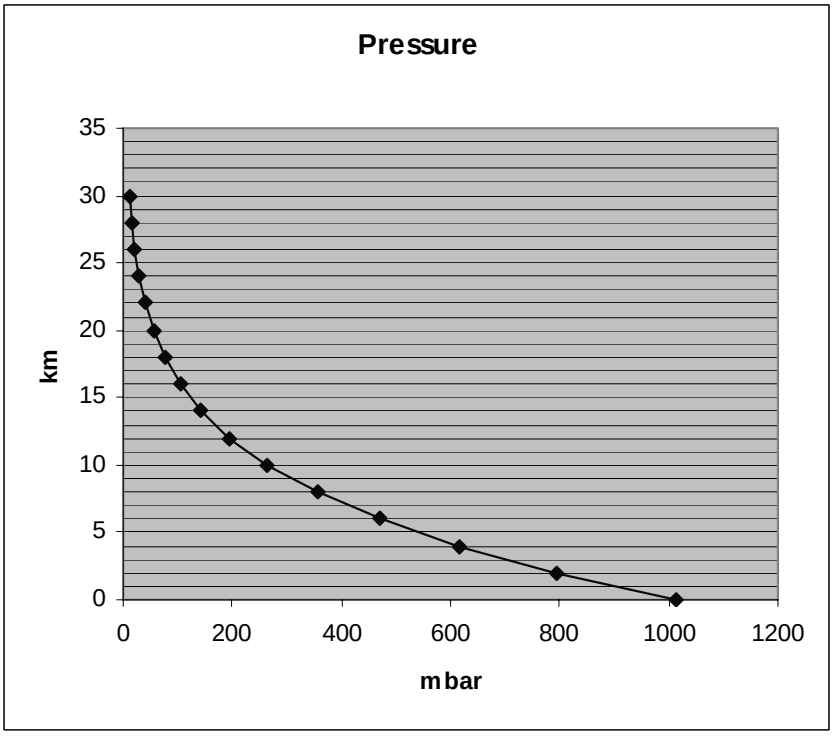
Pressure
35
30
25
20
15
10
5
0
km
0
200
400
600
800
1000
1200
mbar

(b)

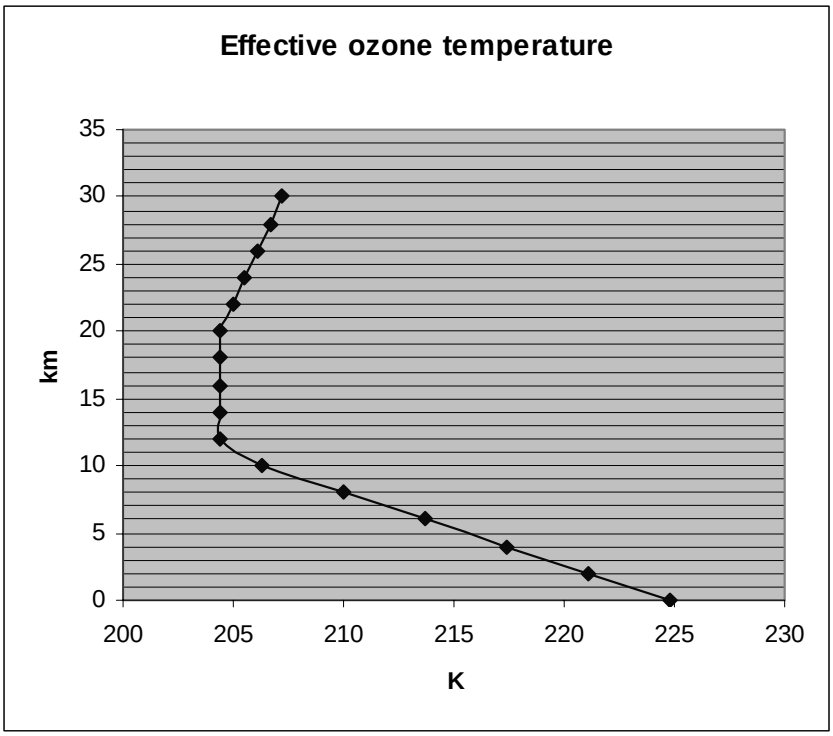
Effective ozone temperature
35
30
25
20
15
10
5
0
km
200
205
210
215
220
225
230
K

(c)

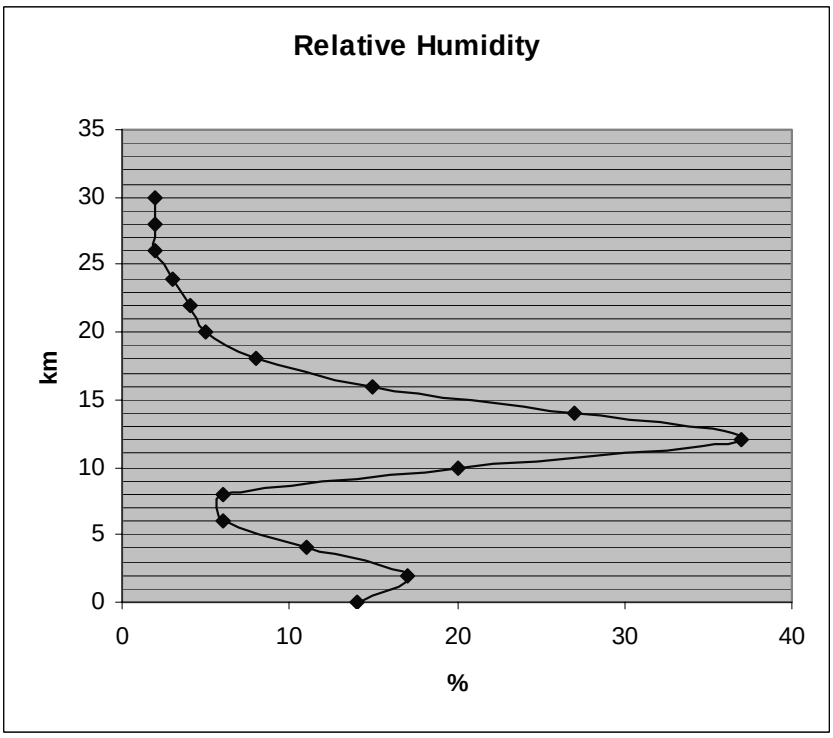
Relative Humidity
35
30
25
20
15
10
5
0
km
0
10
20
30
40
%

(d)

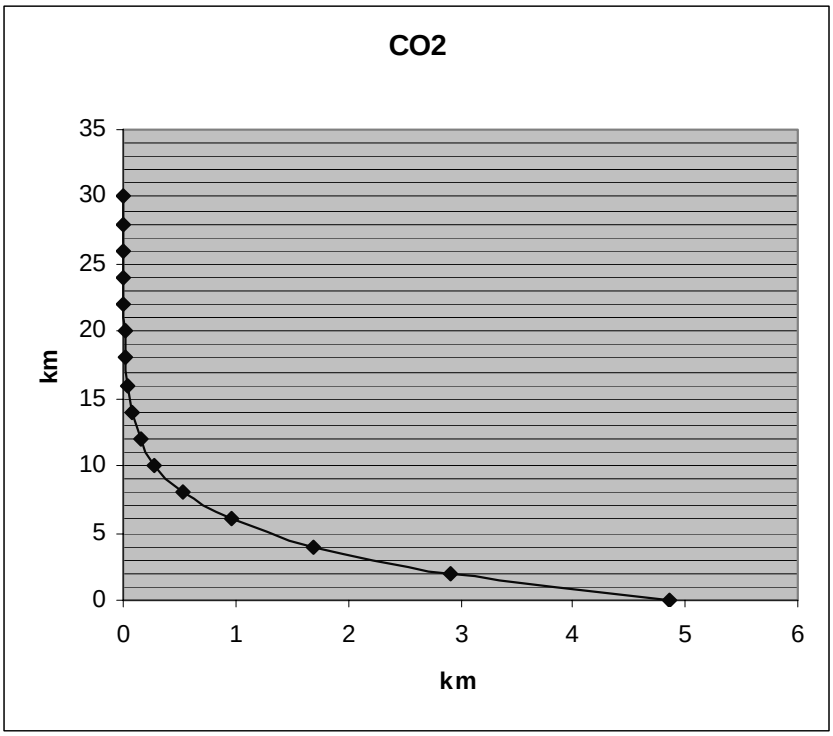
CO2
35
30
25
20
15
10
5
0
km
0
1
2
3
4
5
6
km

(e)

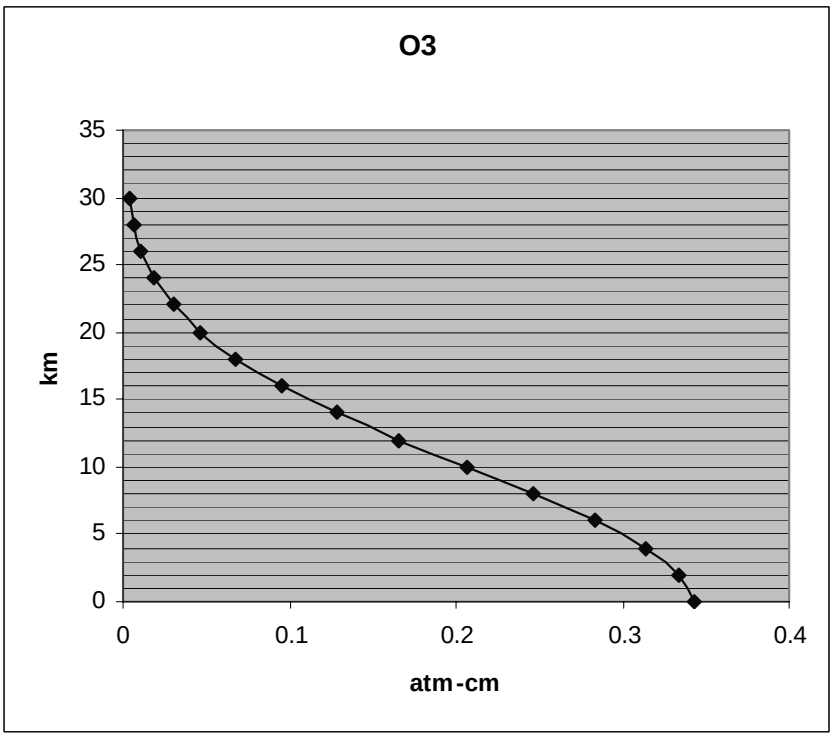
O3
35
30
25
20
15
10
5
0
km
0
0.1
0.2
0.3
0.4
atm-cm

(f)

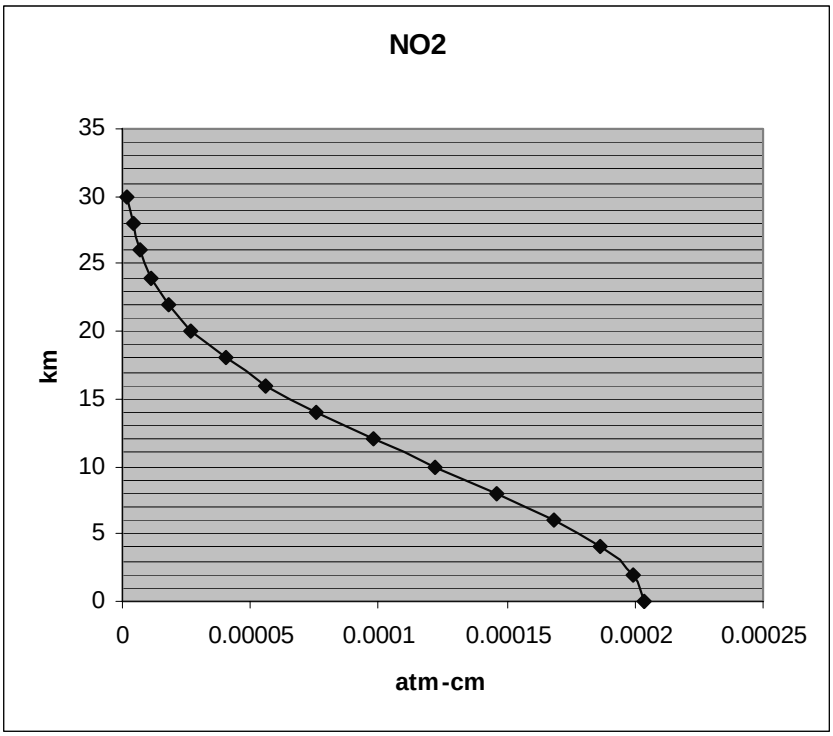
NO2
35
30
25
20
15
10
5
0
km
0
0.00005
0.0001
0.00015
0.0002
0.00025
atm-cm

(g)

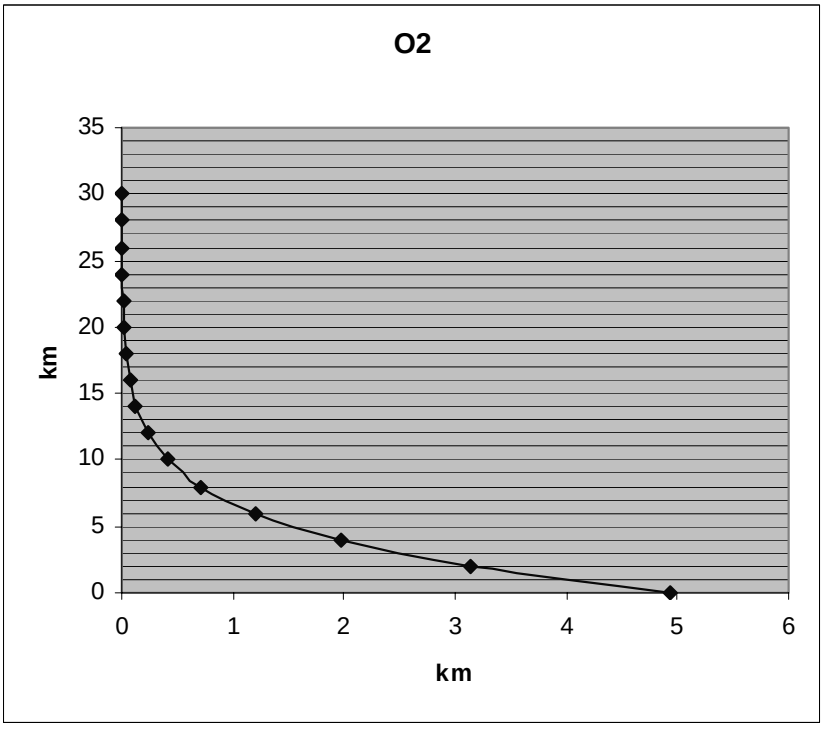
O2
35
30
25
20
15
10
5
0
km
0
1
2
3
4
5
6
km

(h)

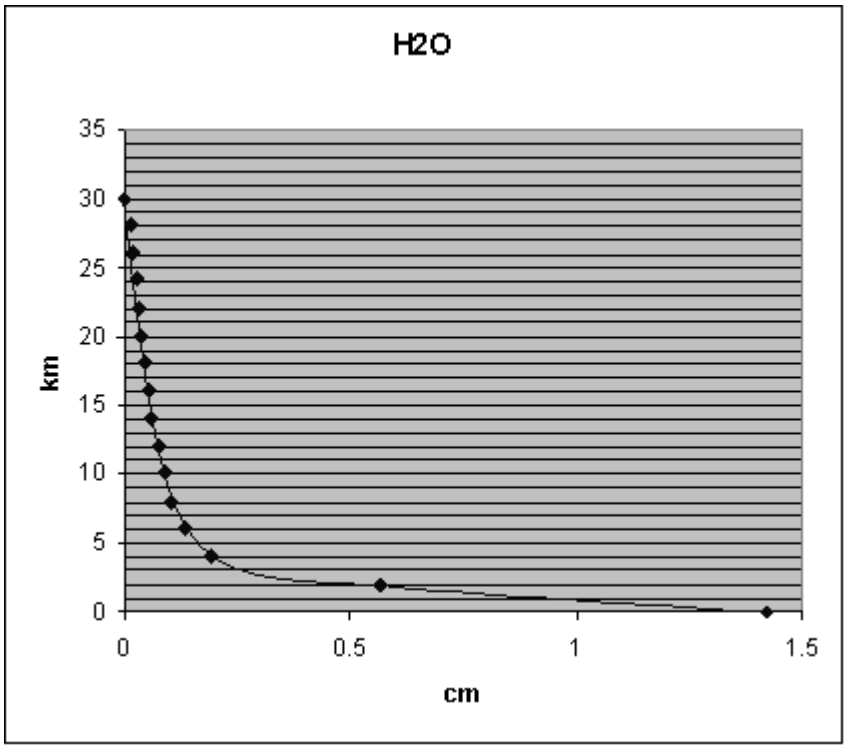

(i)

Figure 3.4 Atmospheric vertical profiles (a)-(d) and effective path lengths (e)–(i) vs. altitude.

The first two vertical profile coefficients: T_a and p were obtained directly from the U.S. Standard Atmosphere (McCartney, 1976). The other two: T_{eo} and RH are not provided by the cited reference, therefore are needed to be obtained from somewhere else. According to (Gueymard, 1995), a correlation (see Equation 3.7) can be used in conjunction with T_a to obtain the approximation of T_{eo}.

$$T_{eo} = 142.68 + 0.28498 \times T_a \tag{3.7}$$

RH is calculated using a standard mathematical formula (see Equation 3.8) taken from the scientific literature. Actual vapour pressure and saturation vapour pressure at each altitude are calculated using the dew point values tabulated by McKenna et al (2003).

$$RH = \frac{actual\ \ vapour\ \ pressure}{saturation\ \ vapour\ \ pressure} \times 100\% \tag{3.8}$$

$$Saturation\ \ vapor\ \ pressure = 6.11 \times 10.0^{\left[7.5 \times Air\ \ Temperature / \left(237.7 + Air\ \ Temperature\right)\right]} \tag{3.9}$$

$$Actual\ \ vapor\ \ pressure = 6.11 \times 10.0^{\left[7.5 \times Dew\ \ Point / \left(237.7 + Dew\ \ Point\right)\right]} \tag{3.10}$$

Effective path length coefficients were each obtained using different methods. O_2 and CO_2 scale heights are calculated as a function (see Equation 3.11) of pressure and air temperature where $P = p/p_0$, and $\theta = 288.15/T$ (Gueymard, 1995). The coefficients take the following values for O_2: $c_0 = 4.9293km$, $c_1 = 1.8849$, $c_0 = 0.1815$, and for CO_2: $c_0 = 4.8649km$, $c_1 = 1.9908$, $c_0 = -0.697$.

$$u_g = c_0 P^{c1} \theta^{c2} \tag{3.11}$$

As for O_3 and NO_2, Gueymard (1995) provided the C_t factor which help corrects their ground-level total abundance values with respect to altitude z in km.

$$C_t = 1 - 0.00898z \tag{3.12}$$

Finally, H_2O or total precipitable water above each level was obtained using the Simpson's rule of integration whereas the incremental precipitable water Δw, for an incremental atmospheric column of height Δz, is calculated using (Gueymard, 1995):

$$\Delta w = \rho_v \Delta z \tag{3.13}$$

The above functions were used to calculate both atmospheric vertical profile and effective path length at each altitude increment of 2km. The resulting graphs are shown in Figure 3.4.

3.3.2 Producing the All-Sky (Spectral Irradiance) Maps for Each Reference Layer

The next task was to utilize the completed atmospheric profile with SMARTS2 model to produce the sky (spectral irradiance) map for each possible sky condition. First, five altitude points that best captured the density changes within the 30km range are identified. Only five are required since the vertical atmospheric profile and effective path length within this range can be interpolated exponentially with pressure (Gueymard, 1995).

Using these graphs as a rough guide (see Figure 3.4), in which these coefficients were plotted against altitude; the five pressure points were identified as 0km, 6km, 12km, 20km, and 30km. These five altitudes best captured the shape of the curve/spline for all the nine graphs. They may or may not captured exactly all the data points shown in the graphs but the aim here is just to capture the rough shape of the density vs. altitude curve. The reference altitude's atmospheric profiles are tabulated in Table 3.1.

Table 3.1 Vertical profiles (a) and effective path lengths (b) at each reference altitude**.**

z	**Vertical profiles**			
	T_a	p	T_{eo}	RH
(km)	**(K)**	**(mb)**	**(K)**	**(%)**
0	288.1	1013.3	224.8	14
6	249.2	472.2	213.69	6
12	216.6	194	204.42	37
20	216.6	55.29	204.42	5
30	226.5	11.97	207.23	2

(a)

z	**Effective path lengths**			
	O_2	CO_2	H_2O	O_3
(km)	**(km)**	**(km)**	**(cm)**	**(atm-cm)**
0	4.9293	4.8649	0.38560	0.3434
6	1.2	0.9614	0.07051	0.3249
12	0.2302	0.1484	0.03489	0.3064
20	0.0216	0.0122	0.00471	0.2817
30	0.0012	0.0006	0.00337	0.2509

(b)

The above table were used with SMARTS2 to produce seventy-five sky (spectral irradiance) distribution maps. This is the result of a combination between five reference altitude values, three turbidity values and five sun positions. The above combination was devised in such way to capture all-type of daylight skies at each reference layer (altitude) of the Earth's atmosphere, using the lowest amount of parameters as possible.

An example of the sky distribution map is shown in Figure 3.5 below. The map contains 271 endpoints; each with a zenith increment of 10° and azimuth increment of 12° respectively.

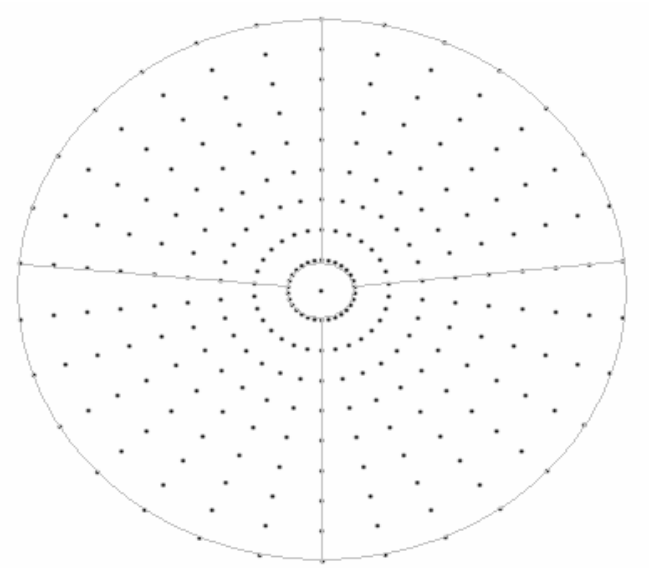

Figure 3.5 Sky distribution map containing 271 endpoints.

3.3.3 Converting the All-Sky (Spectral Irradiance) Maps' Unit to Yxy

The produced sky (spectral irradiance) maps' unit are then converted to the Yxy-colour space. The purpose behind this conversion is to prepare the maps for the fitting process; described in the last section of this chapter. The procedures involved were as follows: i) convert each endpoint's spectral irradiance to the XYZ colour space and ii) transform XYZ to Yxy. Standard CIE-approved algorithms were used (Poynton, 1995). These algorithms are presented in a pseudocode form in Chapter 4.

3.3.4 Producing a Look-Up Table by Fitting the All-Sky (Yxy) Maps to a Parametric Function

The parametric luminance function chosen for the fitting process is Perez et al's (1993) formulation. This formulation has been battle-tested and has few enough

variables so that the optimization stage of the fitting process is likely to converge. (Perez et al's, 1993) formulation was selected in preference to the CIE models (CIE, 1994) because it has a slightly more general form; thus capturing more features of the simulated data.

According to (Preetham et al, 1999), (Perez et al's, 1993) formulation is a poor way to represent CIE X and Z variables, nevertheless the chromaticity x and y are well represented, hence the reason of using Yxy instead of the XYZ-colour space. Chromaticity x and y are similarly behaved, thus are given by the same model with luminance Y (Preetham et al, 1999). A look-up table as a function of turbidity and sun position was duly obtained. It relates the five parameters values for Y, x and y with the turbidity and the sun position at each reference altitude. Zenith's Yxy values for each sky distribution map were also tabulated. The fitting process was performed using the Levenberg-Marquardt non-linear least squares method provided in the MATLAB Optimization Toolbox (Grace, 1992).

CHAPTER 4

IMPLEMENTATION

4.1 Introduction

This chapter describes the implementation of the proposed research methodology. The first module (pre-processing) is described first, followed by the second module (run-time processing). The second module was implemented using OpenGL's GLUT library with the *ARB_fragment_program* extension. As a result, a pixel/vertex-based shader program containing the proposed real-time rendering engine was successfully developed. It was written and compiled using nVIDIA's high-level shader programming language, Cg. The pixel/vertex-based shader is then integrated into a flight simulator prototype system; completes with terrain and a hemispherical sky dome rendering for evaluation purposes.

4.2 Pre-Processing Module

4.2.1 Simulation Phase

The purpose of the simulation phase was to prepare the all-sky colour distribution maps. These maps were the result of the simulation performed with Gueymard's (1995) SMARTS2 model with the developed general atmosphere profile

described in Section 3.3.1. The simulation was carried out on a combination between five reference altitudes, three turbidity values and five sun positions. Each map contains a total of 271 individual endpoints; their spectral irradiance is approximated first using SMARTS2 before being converted to the Yxy-colour space. The simulation's pseudocode is given by:

```
1.0   FOR each reference layer

      1.1   FOR each turbidity

            1.1.1 FOR each sun position

                  1.1.1.1     FOR each endpoint
                        1.1.1.1.1   IF zenith-direction endpoint
                              1.1.1.1.1.1 Use SMARTS2 to calculate
                                    spectral irradiance
                        1.1.1.1.2   ELSE
                              1.1.1.1.2.1 Use the transition model
                                    option to calculate spectral
                                    irradiance

                  1.1.1.2     FOR each endpoint
                        1.1.1.2.1   Convert spectral irradiance to
                                 XYZ
                        1.1.1.2.2   Convert XYZ to Yxy
                        1.1.1.2.3   Assign Yxy to the current
                                 endpoint
```

Figure 4.1 Pseudocode for the simulation task.

The two colour space conversions involved in the above pseudocode were performed using the standard formulations obtained from (Poynton, 1995). The pseudocode for XYZ to Yxy is given by,

```
1.0   Y = Y
2.0   x = X / (X + Y + Z)
3.0   y = Y / (X + Y + Z)
```

Figure 4.2 Pseudocode for the conversion of XYZ to Yxy.

The pseudocode for spectral irradiance to XYZ is given by,

```
1.0   FOR each wavelength λ
      1.1   normalizing constant(λ) = D65 illuminant(λ) x CIE
            matching function(λ).y
      1.2   D65INC(λ) = D65 illuminant(λ) x normalizing
            constant(λ)
      1.3   X += spectral data(λ) x (CIE matching function(λ).x
            x D65INC(λ))
      1.4   Y += spectral data(λ) x (CIE matching function(λ).y
            x D65INC(λ))
      1.5   Z += spectral data(λ) x (CIE matching function(λ).z
            x D65INC(λ))
      1.6   K += CIE matching function(λ).y

2.0   X = X / K
3.0   Y = Y / K
4.0   Z = Z / K
```

Figure 4.3 Pseudocode for the conversion of spectral irradiance to XYZ.

4.2.2 Statistical Fitting Phase

```
1.0   FOR each sky colour (Yxy) distribution map
      1.1   Store zenith's Yxy in the look-up table

      1.2   FOR component-Y
            1.2.1 Fit all endpoints' luminance Y values to the Perez
                  et al (1993) function
            1.2.2 Store the resulting ABCDE values to the look-up
                  table

      1.3   FOR component-x
            1.3.1 Fit all endpoints' chromaticity x values to the
                  Perez et al (1993) function
            1.3.2 Store the resulting ABCDE values to the look-up
                  table

      1.4   FOR component-y
            1.4.1 Fit all endpoints' chromaticity y values to the
                  Perez et al (1993) function
            1.4.2 Store the resulting ABCDE values to the look-up
                  table
```

Figure 4.4 Pseudocode for the statistical fitting task.

The purpose of the statistical fitting phase was to prepare a look-up table; containing the (Perez et al's, 1993) five parameters values for each i) component-Y, ii) component-x and iii) component-y of the Yxy-colour space. As expected, a total of 75 entries for the look-up table were duly obtained; corresponding to the amount of the sky colour distribution maps produced from the previous simulation phase. These entries were obtained by fitting each map to the (Perez et al's, 1993) parametric formulation using the Levenberg-Marquardt non-linear least squares method (Levenberg, 1944 and Marquardt 1963), provided in the MATLAB's Optimization Toolbox. The pseudocode for the statistical fitting task is given in Figure 4.4. The ensuing look-up table is given in Appendix A.

4.3 Run-Time Processing Module

This module describes the workflow of the real-time rendering engine. The engine was implemented on top of a flight simulator prototype system; completes with a hemispherical sky dome and terrain rendering. The terrain and the sky dome were merely abstract data. If rendered without the atmospheric effects, the terrain will be without its sense of scale and distance. The sky dome will also stay in its initial colour, which is pure black (the colour of the outer space).

Using the pixel/vertex-based shader capability of the newer nVIDIA's graphic cards, the atmospheric effects function can be easily integrated into the graphical rendering pipeline. Hence, the function will be performed on each pixel or vertex that was passed on to the OpenGL API.

The real-time rendering engine consists of a series of steps. These steps are executed sequentially each time *glutDisplayFunc()* is requested. The pseudocode for the real-time rendering engine is given by,

```
1.0   FOR each pixel or vertex passed to the OpenGL API

      1.1   Assign pixel/vertex's texture colour, colour, to RGB_obj

      1.2   Perform is_it_skydome_endpoints() function
            1.2.1 IF yes
                  1.2.1.1     Set flag as sky dome endpoint
                  1.2.1.2     Set transparency σ as zero
            1.2.2 IF no
                  1.2.2.1     Set flag as distant object
                  1.2.2.2     Perform calculate_transparency()

      1.3   Perform assign_RGBatm()

      1.4   Calculate  RGB_pv = σ RGB_obj + (1 − σ) RGB_atm

      1.5   Return RGB_pv
```

Figure 4.5 Pseudocode for the real-time rendering engine.

The above pseudocode (see Figure 4.5) was implemented as a pixel/vertex-based shader; written and compiled using Cg. It receives input in the form of a single structure, *pixel_in*,

```
struct  pixel_in  {
     float3  colour     :  COLOUR0;
     float3  texcoord   :  TEXCOORD0;
     float3  camcoord   :  TEXCOORD1;
     float3  skyparam   :  TEXCOORD2;
)
```

The *pixel_in* structure contains four three-dimensional vectors named *colour*, *texcoord*, *camcoord* and *skyparam*. The "COLOUR0", "TEXCOORD0", "TEXCOORD1" and "TEXCOORD2" labels are called binding semantics; they simply indicate the type of data that each variable represents. For example, "TEXCOORD0" represents the texture coordinates for the first texture unit and it is associated with the *texcoord* variable. Thus, the *texcoord* variable contains the first texture unit's texture coordinates; representing the current pixel/vertex's coordinates. As for the other three 3D vectors, *colour* represents the current pixel/vertex's RGB-colour and *camcoord* contains the current camera/observer's coordinates. As for the *skyparam* vector, *skyparam[0]* contains the current turbidity value, *skyparam[1]*

contains the current sun zenith angle and *skyinfo[2]* contains the current sun azimuth angle.

The shader also returns output in the form of a single structure, *pixel_out*. It contains the final RGB-colour of the pixel/vertex that will be rendered to the scene.

```
struct  pixel_out  {
     float3  colour    :  COLOUR;
)
```

There are three function calls made in the above pseudocode (see Figure 4.5). The first function call (Step 1.2) is to check whether the current pixel/vertex coordinates match any of the stored sky dome global coordinates. The second function call (Step 1.2.2.2) is to calculate the transparency value for the current viewing path (for camera - distant object only). The third function call (Step 1.3) is to assign the correct RGB_{atm} value for the current viewing path. The following three sub-sections are dedicated for explaining the three functions comprehensively.

4.3.1 The *is_it_skydome_endpoints()* Function

As explained earlier in Chapter 1, the sky dome is a hemispherical structure that "follows" the camera (observer) movement. Each sky dome endpoint has its own initial (local) coordinates (see Figure 4.6) with the camera (observer) positioned at the centre (0, 0, 0). These coordinates must be updated each time the camera moves. The new coordinates are then stored as the global coordinates of the sky dome's endpoints.

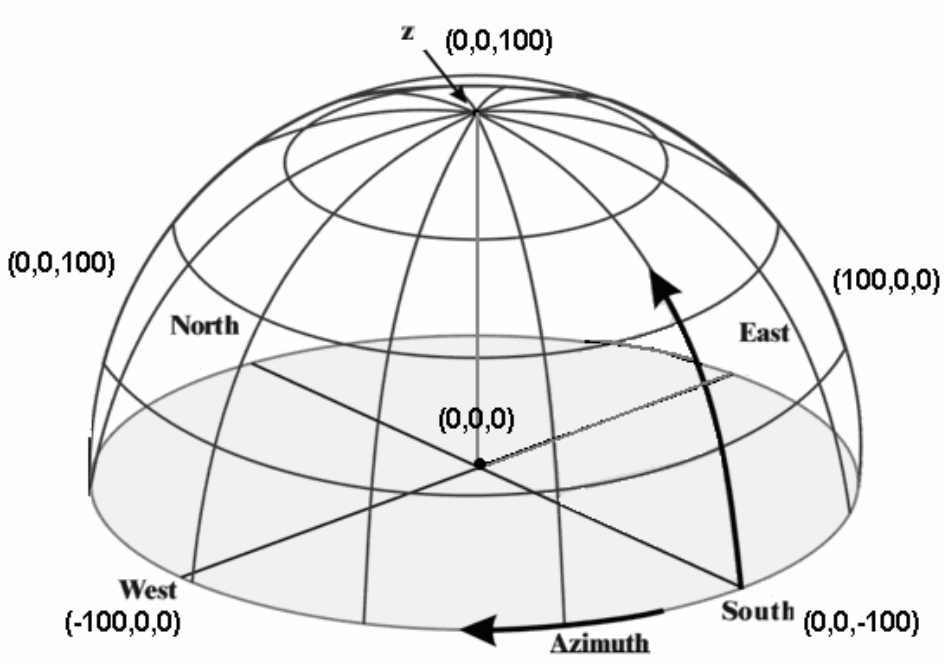

Figure 4.6 The sky dome initial coordinates, obtained from its 3DS ASCII file.

Note that these global coordinates are only updated if the camera is moving on the x-axis and z-axis. Any movement on the y-axis would not cause the sky dome endpoints' global coordinates to be updated. This is to allow the above-ground flying situation to be simulated, so the pilot will be able to observe the lower sky horizon line from his or her current flight altitude. Note that the maximum y-axis value is limited to 30 units (1 unit is equivalent to 1 km) since the permissible flying altitude is only up to 30km.

Each sky dome endpoint's information is stored in an array of a single structure, *skydome_endp*,

```
struct  skydome_endp  {
     float   R              :  RED;
     float   G              :  GREEN;
     float   B              :  BLUE;
     float3  globalcoord    :  ENDPCOORD;
)
```

The global coordinates of each endpoint are updated each time the camera moves along the x-axis and z-axis. The pseudocode for updating the endpoints' global coordinates is given by,

```
1.0   addx = camera.x
2.0   addz = camera.z

3.0   FOR each sky dome endpoints
      3.1   globalcoord[0] = globalcoord[0] + addx
      3.2   globalcoord[2] = globalcoord[2] + addz
```

Figure 4.7 Pseudocode for updating the sky dome endpoints' global coordinates.

The pseudocode given above is self-explanatory. The current camera global coordinates are obtained from the variable *camcoord* in the *pixel_in* structure. The camera's global point-x and point-z describe the amount of transitional unit needed to be added to each sky dome endpoint's current global coordinates. To check whether the current pixel or vertex, *texcoord*, is indeed a sky dome endpoint (unobstructed viewing path), simply run a test to find out if the given coordinates match any of the updated sky dome endpoints' global coordinates.

4.3.2 The *calculate_transparency()* Function

This function calculates the transparency value of the given obstructed viewing path. The function is based on the discussion done in Section 3.2.1.1. The pseudocode is given by,

```
1.0   z1 = camera.y
2.0   z2 = pixel/vertex.y

3.0   Scale z1 and z2

4.0   IF abs(z2 – z1) > 1.0
      4.1   Calculate optical depth, τ = (1/(z2 – z1))(– e^(–z1) – e^(–z2))
      4.2   Calculate transparency, σ = e^(–τ)
      4.3   RETURN transparency
5.0   ELSE
      5.1   Calculate extinction coefficient, ε = e^(–z1)
      5.2   Calculate transparency, σ = e^(–εδ)
      5.3   RETURN transparency
```

Figure 4.8 Pseudocode for calculating the transparency value.

4.3.3 The *assign_RGBatm()* Function

This function assigns the correct RGB_{atm} for the current viewing path (camera – pixel/vertex). There are two steps involved in this function: i) prepare the current layer's sky colour distribution map using the exponential atmospheric colour contribution (RGB_{atm}) model and ii) associate the current viewing path to the correct sky dome endpoint (RGB_{atm}).

4.3.3.1 Exponential RGB_{atm} model

This model implementation is based on the discussion done in Section 3.2.2.2. The pseudocode is given by,

```
1.0   Get the current turbidity, skyinfo[0]
2.0   Get the current sun zenith, skyinfo[1]
3.0   Get the current sun azimuth, skyinfo[2]

4.0   Prepare the five reference layers' current sky map
      4.1   FOR each reference layer's sky map
            4.1.1 FOR each endpoint on the sky map
                  4.1.1.1     Get current ABCDE values
                  4.1.1.2     Calculate Yxy using the Perez Function
                  4.1.1.3     Store the Yxy value

5.0   Get the current observer's altitude

6.0   Prepare the current layer's sky map
      6.1   FOR each endpoint on the sky map
            6.1.1 Interpolate the value from the five similar
                  endpoints
            6.1.2 Convert Yxy to RGB
            6.1.3 Store the RGB value
```

Figure 4.9 Pseudocode for the exponential RGB_{atm} model.

The pseudocode for Yxy to RGB is given by,

```
1.0   Convert Yxy to XYZ
      1.1   X = x * ( Y / y )
      1.2   Y = Y
      1.3   Z = ( 1 - x - y ) * ( Y / y )
2.0   Convert XYZ to RGB
      2.1   R = (3.240479 * X) + (-1.537150 * X) + (-0.498535 * X)
      2.2   G = (-0.969256 * Y) + (1.875992 * Y) + (0.041556 * Y)
      2.3   B = (0.055648 * Z) + (-0.204043 * Z) + (1.057311 * Z)
```

Figure 4.10 Pseudocode for the conversion of Yxy to RGB.

4.3.3.2 Association Test

This test is carried out to determine which endpoint is currently being intersected by or associated with the viewing path. The association test is based on the discussion done in Section 3.2.2.2. The pseudocode is given by,

```
1.0   FOR each sky dome endpoint's global coordinates
      1.1   Assign camcoord as P0
      1.2   Assign texcoord as P1

      1.3   Calculate t_all, by solving the first component,
            t_all = (x − x0)/(x1 − x0)

      1.4   Replace t with t_all
            1.4.1 IF  y − (y0 + (y1 − y0)t_all)  < error_boundary
                  1.4.1.1     Set FLAG1 as true
            1.4.2 IF  z − (z0 + (z1 − z0)t_all)  < error_boundary
                  1.4.2.1     Set FLAG2 as true

      1.5   IF both FLAG1 AND FLAG2 are true
            1.5.1 Assign current endpoint's RGB as RGBatm
            1.5.2 EXIT LOOP
```

Figure 4.11 Pseudocode for calculating the association test.

CHAPTER 5

RESULTS AND ANALYSIS

5.1 Introduction

This chapter serves two purposes: i) presents and evaluates the test results as well as ii) compares the proposed model performance against the previous real-time aerial perspective methods, namely (Nielsen, 2003) and (Hoffman and Preetham, 2002).

First, the evaluation was done by comparing a series of rendered test scenes with actual images of the daylight skies. These scenes were purposely picked to demonstrate the proposed system properties: i) the ability to capture the sky colour with changing sun position, ii) the ability to capture the sky colour with changing turbidity, iii) the ability to capture the increase in intensity as the view approaches the sun, iv) the ability to render correct sky colour distribution at different observer altitude and lastly, v) the ability to capture the aerial perspective effects on distant objects correctly.

This non-scientific evaluation technique is employed by both previous real-time aerial perspective methods (Hoffman and Preetham, 2002 and Nielsen, 2003). The rendered atmospheric effects (sky and distant objects) are only required to visually-convince the pilot (Nielsen, 2003); not to match the equivalent actual image pixel-by-pixel. The term “equivalent” itself is almost impossible to achieve. It will be an arduous task to measure every existing parameter that influences the atmospheric effects

whenever an actual image of the daylight sky or a distant object is taken. Even if that is possible, the non-availability of the scientific measuring equipments during this research prohibits such tasks to be carried out. Also, it must be pointed out that a numerical model cannot be validated or verified, despite the frequent usage of these terms in this field, because of the fundamental reasons critically reviewed by Oreskes et al. (1994). For these reasons above, the non-scientific evaluation technique, by comparing two (rendered vs. actual) images side-by-side, mentioned earlier is considered as sufficient for this research context.

Second, the proposed model performance was compared against Nielsen's (2003) and Hoffman and Preetham's (2002) results. Several criteria are taken into consideration: i) the existence of visual flaws and ii) the frame rate.

5.2 System Specifications

The flight simulator prototype system was run using these software and hardware specifications (see Table 5.1 and Table 5.2). All previous methods used during the comparison task were also run using this current testbed. This means that, the frame rate results obtained by all three models are dependent on these hardware and software specifications.

Table 5.1 Hardware specifications.

Hardware	Specification
Motherboard	Gigabyte GA-74400-L1 (AGP 8x)
Processor	AMD Athlon XP 1800+ (1.53 GHz)
Main memory (RAM)	1 GB DDR400 Kingston
Graphics card	Asus nVIDIA GeForce FX 5700 (256 MB, 128-bit, AGP 8x)

Table 5.2 Software specifications.

Software	Specification
Operating system	Microsoft Windows XP Professional (Service Pack 1)
Development tools	Microsoft Visual C++ 6.0 nVIDIA Cg Compiler 1.4 MATLAB 7.0
Graphics library	OpenGL 1.2

5.3 Evaluation

To validate the proposed model as a legit atmospheric effects rendering method, a series of test scenes were rendered and compared with actual images of the daylight skies. Five criteria, as suggested by Nielsen (2003), were chosen as the evaluation parameters. The first four are categorized under the daylight sky colour properties. The last criterion is categorized under the aerial perspective effects property.

5.3.1 Daylight Sky Colour

5.3.1.1 Sky Colour With Changing Sun Positions

The colour and intensity of the sky change during the day. This effect is most noticeable during sunrise and sunset. Figure 5.1 below shows the results of rendering the daylight sky colour at different sun positions using the proposed model. These images were rendered with the turbidity set to low.

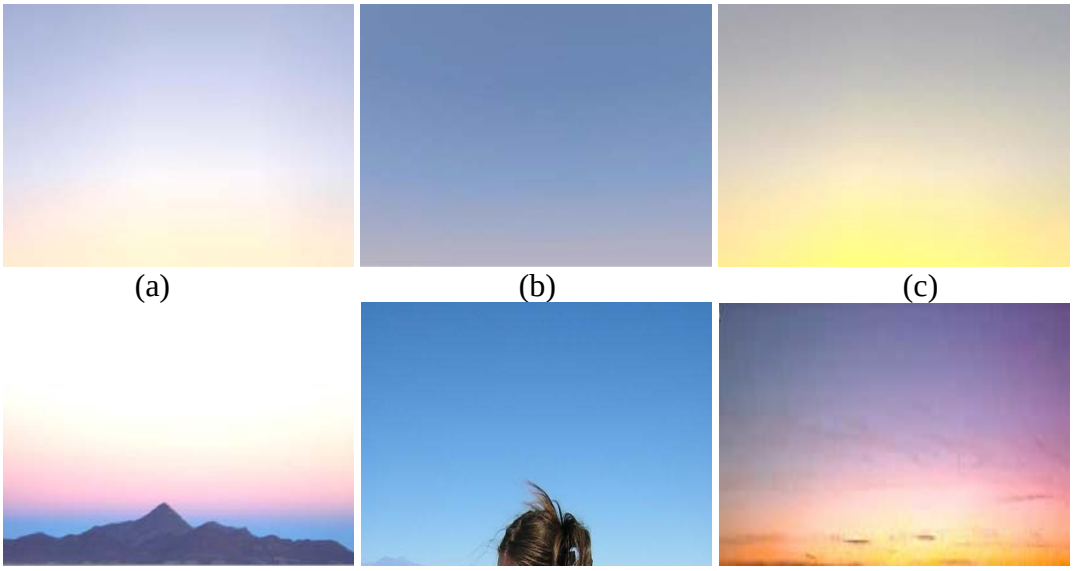

(a) (b) (c)

(d) (e) (f)

Figure 5.1 Rendered skies at: a) sunrise, b) mid-noon and c) sunset. Actual images of the skies at: d) sunrise, e) mid-noon and f) sunset.

5.3.1.2 Sky Colour With Changing Turbidity

Notice the differences between the rendered sky images in Figure 5.2 (a) and Figure 5.2 (b).

(a) (b) (c)

Figure 5.2 Rendered sky with: a) low turbidity and b) high turbidity. An actual image of a turbid sky c) is included for evaluation purposes.

Sky with higher turbidity (see Figure 5.2 (a)) seems to be almost isotropic; compared to the less turbid sky (see Figure 5.2 (b)) whereby the colour contrast is much more

apparent between the horizon and the zenith. The sky also whitens excessively due to the large presence of Mie scatterers (aerosols) in the air.

5.3.1.3 Intensity of the Sky Area Close to the Sun

The intensity (approaching white) increases rapidly as the view approaches the sun. This is the result of the Mie scattering phase function. This effect can be seen in Figure 5.3.

(a) (b)

Figure 5.3 Sky colour, either a) rendered or b) from an actual image, at area close to the sun.

5.3.1.4 Sky Colour Distribution With Respect to the Observer's Altitude

In both the images rendered by the proposed system (Figure 5.4 (a)-(c)) and the images taken of the real atmosphere at different altitudes (Figure 5.4 (d)-(f)), it can be seen that the colour of the horizon stays white and bright regardless of the observer altitude. It can also be seen that the sky closer to zenith gets darker with increased observer altitude.

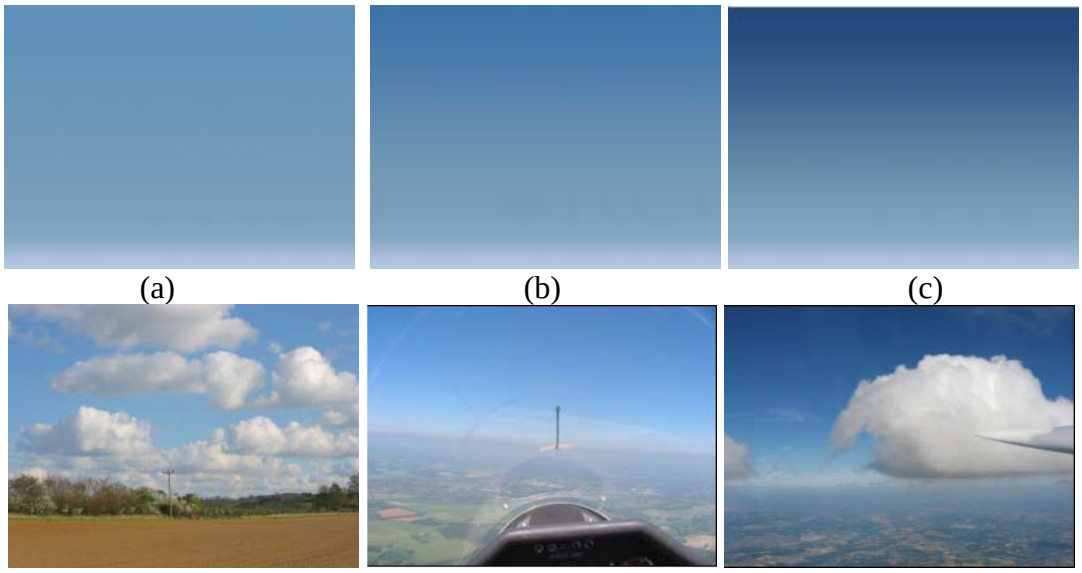

(a) (b) (c)

(d) (e) f)

Figure 5.4 Rendered sky images viewed from: a) 0km, b) 5km and c) 10km. Actual sky images viewed from: d) 0km, e) 5km and f) 10km.

5.3.2 Aerial Perspective Effects

The pixel/vertex-based shader was implemented on top of a virtual world, completes with terrains and a hemispherical sky dome rendering. Without the atmospheric effects, the scene looks dull and uninteresting (see Figure 5.5 (b)). There is no clear indicator of scale and distance. Closer terrains have no noticeable differences in appearance if compared to distance terrains.

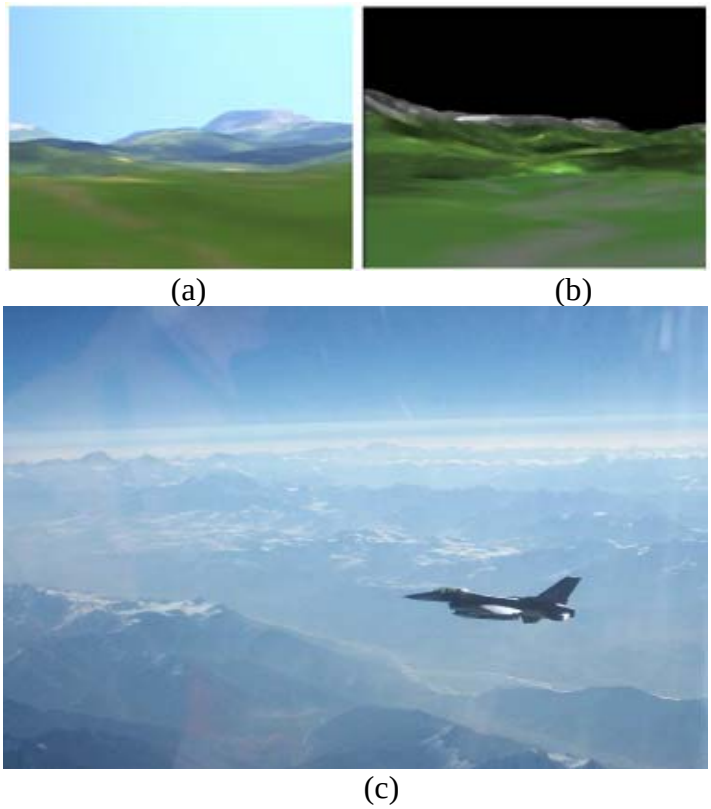

(a) (b)

(c)

Figure 5.5 The rendered scene with a) and b) without the atmospheric effects. An (c) actual image depicting the atmospheric effects is also shown for comparison purpose.

As can be seen in Figure 5.5 (b) the two atmospheric effects: i) loss in contrast and ii) colour shifts are missing. The sky dome stays as its initial colour: black. Now, let's examines the rendered scene in Figure 5.5 (a) whereas the pixel/vertex-based shader is activated. Notice that the two atmospheric effects: i) loss in contrast and ii) colour shifts with distance, are well captured. The bright mountain peak's colour shifted to red whilst the darker mountain peak's colour shifted to blue as the distance increased. The distance terrain also exhibited noticeable contrast loss and appeared to be blending in with the horizon.

5.4 Comparison

The two criteria chosen as the comparison parameters are: i) the existence of visual flaws and ii) the rendering frame rate.

For the first criterion, these two visual flaws were checked whether they too existed in the proposed model's results: i) the absence of faint blue colour at the zenith sky during low sun altitudes, due to the absence of the ozone absorption contribution (Minnaert, 1954) and ii) the exaggerated visible dark band, appearing at the sky area perpendicular to the sun, due to the naive direct mapping from intensity values to RGB (Nielsen, 2003).

The second criterion, the rendering frame rate is compared for all three models. Since all three were implemented as a pixel/vertex-based shader, the comparison is made easy by testing all of them on a single terrain dataset.

5.4.1 The Existence of Visual Flaws

5.4.1.1 The Absence of Faint Blue Colour at the Zenith Sky during Lower Sun Altitudes

Figure 5.6 (a) shows the sample image rendered using Nielsen's (2003) method. The second image (see Figure 5.6 (b)) was rendered using the proposed model. Both images were rendered at the ground level (0km) with the sun's zenith angle of 90° and turbidity set to low. An actual image (see Figure 5.6 (c)) of a sunrise sky is also included for comparison purposes.

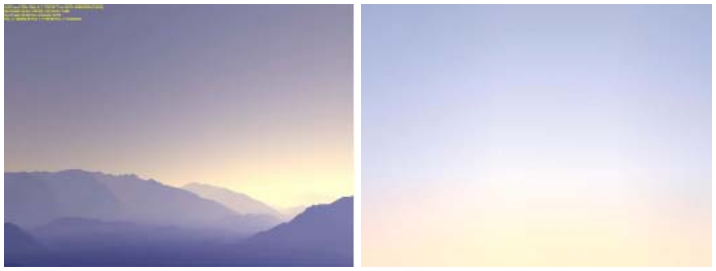

(a) (b)

(c)

Figure 5.6 The “faint blue colour at the zenith sky during low sun altitudes” test.

Based on the rendered images shown above, it can be concluded that the inclusion of absorption or the lack of it does not really influence the amount of blue colour at the zenith sky during low sun altitudes. The motivation to include absorption as a parameter when calculating the light extinction, based on the finding by Minnaert (1954), proved to be futile. In fact, the above rendered results only confirmed the finding by Haltrin (1996) whereas absorption of the visible light is negligible below the ozone layer. However, it is still considered as an achievement for the proposed model to include absorption in its light extinction model. At least, the proposed model can claim to be more physically accurate than the two previous methods.

5.4.1.2 The Exaggerated Visible Dark Band

This visual flaw is reported in Hoffman and Preetham’s (2002) model results (see Figure 5.7 (a)) by Nielsen (2003). Nielsen (2003) corrected the problem by introducing a reduction factor for the Rayleigh scattering phase function. As explained earlier in Chapter 2, the dark band does not exist in the actual world because the high

contrast between the area perpendicular to the sun and its bright neighbouring regions is evened out by the multiple scattering of light. As can be seen in the rendered result shown below (see Figure 5.7 (b)), the proposed model manages to amply reduce the exaggerated dark band effect.

(a) (b)

Figure 5.7 The "exaggerated dark band effect" test.

This is due to the SMARTS2 model, used for calculating the viewing path's spectral irradiance, supporting the multiple scattering of light (Gueymard, 1995).

5.4.2 The Rendering Frame Rate

This comparison task is performed by testing all three methods, implemented as a pixel/vertex-based shader, on top of a single virtual world application. The virtual world application was consisted of a single ROAM terrain dataset and a hemispherical sky dome. By predefining a single camera's path, the average FPS results obtained by each method were tabulated. The results are shown in Figure 5.8.

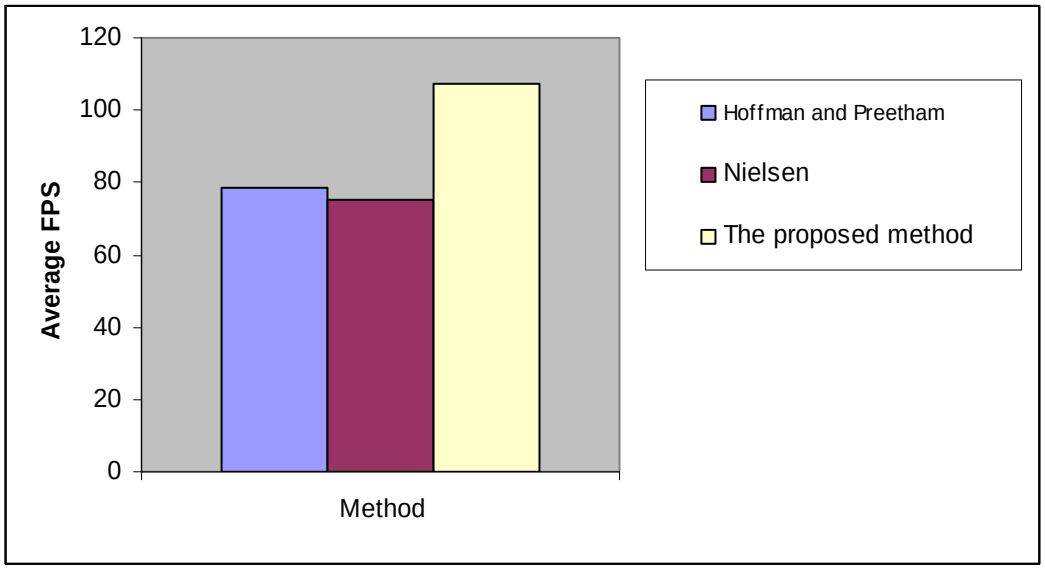

Figure 5.8 The average FPS comparison result.

The proposed method clearly performed better than the two previous real-time aerial perspective methods. It has been proven that the proposed method calculation is far less complex than the real-time aerial-perspective method, yet managed to produce equivalent results. Note that this average FPS value is obtained using a non-optimized implementation of the proposed real-time rendering engine.

5.5 Summary

All of the above results proved that the proposed model is a legit atmospheric effects rendering method. It can render both all-type of daylight skies and aerial perspective effects correctly. Even though the visual results showed not much of an improvement compared to the previous methods but the frame rate obtained using the proposed method is pretty impressive. This is the result of omitting the real-time nested integrals from the pixel and vertex shader operation. The frame rate has the potential of

returning an even more remarkable result if the real-time rendering engine implementation is highly optimized. Besides that, the proposed model also proved its suitability in a flight simulator domain by being capable of simulating correctly the effect of increasing observer's altitude towards the sky colour distribution (the darkening of the sky area close to zenith as the observer's altitude increases).

CHAPTER 6

CONCLUSION

6.1 Conclusion

This research explored the possibility of replacing the real-time calculations involved when solving the current viewing path's LTE with an analytical-based approach. This solved many of the previous real-time aerial perspective methods shortcomings. The offline calculation of the sky colour distribution enabled the physical accuracy of the in scattering and extinction models to be push to the limit. Both multiple scattering and absorption can now be considered during the light transfer calculation; increasing the physical accuracy, hence minimizing the possibility of visual errors. The proposed model is also designed to capture the darkening effect of sky area close to zenith as the observer's altitude increases. This is to ensure that the proposed model is a valid atmospheric effect rendering algorithm in a flight simulator domain. The proposed model is implemented as a pixel/vertex-based shader; allowing it to be integrated seamlessly into the modern graphical rendering pipeline. The research contributions are as follow:

(i) Developed the Earth's general atmosphere profile, up to 30km.
(ii) Produced a look-up table for storing the ABCDE values for Yxy as a function of reference altitude, turbidity and sun position.
(iii) Developed an exponential atmospheric colour contribution model

(iv) Developed an association test algorithm to assign the correct RGB_{atm} to the current viewing path.

(v) Developed a single pixel/vertex-based rendering equation, based on the Beer's Law, to simulate the atmospheric effects on both sky and distant objects (aerial-perspective).

(vi) Applied all of the above models as a real-time rendering engine; implemented as a pixel/vertex-based shader program.

The proposed model is capable of rendering the atmospheric effects on both daylight sky and distant objects. This research can be applied in the following fields:

(i) Computer Games – A computationally efficient method will enable low-end computer to render both sky and aerial perspective effects in an acceptable interactive frame rate. Flight simulator game reaps the most benefits.

(ii) Military/Airline Industry – Help familiarize beginner pilot with the various sky conditions (turbidity level and time setting) as expected to be observed in the real world. Aerial perspective effects helps pilot to judge both scale and distance properly.

(iii) Tourism – Virtual tourism via the "*fly-by*" method.

6.2 Recommendations

There are a few areas of the proposed model that can be improved. Here are the few topic recommendations for the future work:

(i) Optimized the real-time rendering engine

Current real-time rendering engine implementation is not highly optimized. For instance, the sky colour distribution map for each

reference layer does need not to be recalculated every time the camera view changes its orientation (assuming the camera's altitude stay the same). The reference layers' sky distribution maps are required to be updated only if any of these parameters changes: i) camera's altitude, ii) turbidity and iii) sun position. A better optimized algorithm will return a higher FPS performance.

(ii) Applying Tone Mapping Techniques

Currently, the out-of-gamut RGB colour is corrected by reducing the requested colour's saturation until it falls within the possible RGB gamut. Although this method often yields acceptable results, a more physically-correct solution is by using tone mapping. Discussion on the tone mapping techniques can be found in (Ferwerda, 1996; Larson, 1997 and Tumblin, 1993). However, it is unclear how much will the tone mapping technique improves the current results. This additional computation would be an unnecessary burden if the new results did not show any significant improvements.

APPENDIX A

The look-up table displaying the ABCDE value and the zenith Yxy for each combination of reference altitude, turbidity and sun position.

Ref alt	T	(zenith, azimuth)	Coefficients					Zenith		
			A	B	C	D	E	Y	x	y
0km	0.0	90°,90°	-3.57	1.01	0.06	0.44	-0.32	17.34	0.64	0.44
		45°,90°	2.80	0.01	8.09	-0.13	12.11	23.01	1.84	0.89
		0°,0°	1.84	-0.32	7.01	0.19	-4.07	72.3	0.17	0.34
		45°,270°	1.05	5.06	-0.25	0.23	14.77	22.50	0.44	0.64
		90°,270°	-0.13	15.11	2.14	6.44	12.21	16.05	0.77	0.89
	0.5	90°,90°	0.01	-12.20	1.01	34.55	-14.03	19.01	2.14	1.54
		45°,90°	15.11	0.44	8.09	0.01	4.94	25.32	1.11	0.17
		0°,0°	0.19	2.14	12.11	-0.32	-7.02	69.84	5.06	4.03
		45°,270°	0.55	2.06	-0.01	-3.57	5.06	26.14	0.34	0.44
		90°,270°	-0.25	2.80	1.84	1.01	0.07	18.74	0.25	0.22
	1.0	90°,90°	1.05	0.52	3.21	0.55	-14.03	19.89	0.89	1.11
		45°,90°	32.13	0.17	5.06	-4.07	0.01	26.30	1.84	0.39
		0°,0°	0.01	52.07	0.44	-0.25	13.56	54.5	0.17	0.64
		45°,270°	1.01	0.33	16.77	0.19	1.11	26.21	1.11	5.67
		90°,270°	-0.32	2.06	4.08	2.14	-62.03	19.17	2.03	0.44
6km	0.0	90°,90°	-4.07	2.06	22.33	0.52	1.84	19.32	0.17	0.34
		45°,90°	8.09	2.14	-0.30	1.05	30.04	24.03	0.44	2.14
		0°,0°	0.01	0.19	-0.25	15.11	0.44	63.31	0.25	5.06
		45°,270°	1.05	-3.57	4.08	1.84	8.09	23.97	0.64	1.11
		90°,270°	12.11	12.21	5.60	1.01	0.91	19.07	0.34	0.03
	0.5	90°,90°	7.01	-74.10	-0.32	0.01	-4.07	19.03	0.44	0.52

		45°,90°	0.19	0.55	-14.03	0.17	0.44	26.73	0.44	0.25
		0°,0°	-0.01	2.14	-0.25	1.84	9.23	57.04	0.30	0.34
		45°,270°	-7.02	0.01	12.07	-4.07	13.56	25.68	2.06	0.17
		90°,270°	1.01	0.52	-3.57	4.08	-0.13	18.97	0.55	6.44
	1.0	90°,90°	0.07	34.55	2.06	12.21	16.77	18.79	1.11	2.80
		45°,90°	0.01	6.44	22.33	2.80	-0.32	24.76	0.17	0.64
		0°,0°	13.56	1.01	1.05	-62.03	0.19	49.86	0.44	0.89
		45°,270°	2.14	-0.25	15.11	1.01	-0.01	23.45	0.19	0.12
		90°,270°	-3.57	0.01	-4.07	34.55	6.44	18.67	0.64	0.25
12km	0.0	90°,90°	-3.57	-7.02	2.06	32.13	22.12	17.34	0.17	0.55
		45°,90°	7.01	61.02	0.01	13.56	0.17	23.01	0.52	0.64
		0°,0°	34.55	0.44	2.14	0.03	1.84	53.22	5.06	0.17
		45°,270°	5.06	16.77	0.01	-14.03	-0.13	26.21	2.14	0.34
		90°,270°	-0.01	12.11	0.17	2.14	9.23	19.17	2.80	2.06
	0.5	90°,90°	-12.41	1.11	0.19	1.01	8.09	19.01	6.44	0.44
		45°,90°	-0.30	6.44	0.07	0.52	52.07	25.32	8.09	1.84
		0°,0°	-8.70	9.23	0.55	30.04	5.06	48.01	4.45	0.44
		45°,270°	-3.57	2.14	-0.13	16.77	7.01	26.21	4.03	0.19
		90°,270°	13.56	0.55	-0.01	-0.25	-0.32	19.17	0.55	0.17
	1.0	90°,90°	0.19	15.11	30.04	34.55	12.11	18.67	0.89	0.30
		45°,90°	-0.25	12.21	32.13	2.80	2.06	24.55	0.25	0.17
		0°,0°	-62.03	22.12	-7.02	1.01	-0.13	44.77	0.44	2.80
		45°,270°	0.01	2.14	0.19	7.01	-4.07	26.21	0.07	0.25
		90°,270°	-14.03	8.09	-0.30	17.97	1.84	19.17	0.34	1.11
20km	0.0	90°,90°	1.01	32.13	0.55	0.01	9.23	18.64	0.44	0.52
		45°,90°	0.19	-0.25	-0.01	-0.32	1.05	25.12	0.25	5.06
		0°,0°	0.17	0.52	-0.13	13.56	2.14	49.76	4.45	0.44
		45°,270°	0.01	1.01	8.09	5.06	1.11	25.32	0.19	0.89
		90°,270°	5.06	0.07	2.80	61.02	0.19	19.01	8.09	2.06
	0.5	90°,90°	52.07	12.11	0.01	0.17	-4.07	17.34	2.80	6.44
		45°,90°	0.44	9.23	-14.03	2.06	16.77	23.01	0.17	0.17
		0°,0°	0.19	7.01	-8.70	-3.57	-0.01	45.66	1.11	0.64
		45°,270°	-0.13	2.14	34.55	5.06	1.84	26.21	0.34	0.30

		90°,270°	-4.07	2.14	12.11	-0.25	5.06	19.17	1.84	0.19
	1.0	90°,90°	0.17	-0.30	0.32	-0.13	0.19	18.54	4.20	0.52
		45°,90°	1.01	-7.02	1.84	0.07	-0.52	25.67	0.76	0.17
		0°,0°	-14.03	13.56	0.17	0.19	22.12	41.32	0.07	8.09
		45°,270°	-62.03	0.52	15.11	2.06	-14.03	26.08	2.06	4.45
		90°,270°	8.09	-8.70	2.14	13.56	-0.30	18.99	0.19	2.04
30km	0.0	90°,90°	5.06	6.44	-7.02	0.01	-12.08	19.01	1.31	4.03
		45°,90°	12.11	0.07	0.52	13.56	12.21	25.32	6.44	0.19
		0°,0°	1.01	-0.25	2.14	16.77	1.01	44.33	0.52	5.06
		45°,270°	-7.02	0.52	0.17	-14.03	61.02	26.21	4.45	0.89
		90°,270°	-0.13	-0.30	2.06	1.01	-8.70	19.17	0.30	6.54
	0.5	90°,90°	5.13	0.01	1.84	0.07	2.11	23.34	0.50	0.17
		45°,90°	17.97	0.52	5.06	4.45	2.80	19.03	0.19	1.03
		0°,0°	-7.02	1.01	13.56	12.15	-0.13	42.13	0.50	1.31
		45°,270°	8.09	1.01	0.44	0.19	2.14	22.56	8.09	0.75
		90°,270°	22.12	1.05	-0.25	-14.03	1.01	18.77	0.89	0.07
	1.0	90°,90°	5.06	15.11	-2.03	16.77	-7.02	17.34	5.06	2.31
		45°,90°	0.19	-62.03	32.13	0.01	2.06	23.01	0.17	0.52
		0°,0°	61.02	-0.30	7.01	1.01	17.97	39.23	1.31	1.84
		45°,270°	-0.25	-8.70	-4.07	2.14	52.07	26.21	1.76	6.44
		90°,270°	0.44	0.17	1.84	-0.13	-62.03	19.17	0.44	0.50

REFERENCES

Barr A.H. (1991). *Teleological modeling, in making them move: mechanics, control, and animation of articulated figures*, N.I. Badler, B.A. Barsky, and D. Zeltzer, Editors, Morgan Kaufmann, pp. 315-321.

Bird, R. E., and Riordan, C. J. (1986). *Simple Simple Solar Spectral Model for Direct and Diffuse Irradiance on Horizontal and Tilted Planes at the Earth's Surface for Cloudless Atmospheres*. Journal of Climate and Applied Meteorology. Vol. 25(1), pp. 87-97.

Blinn J.F. (1982). *Light Reflection Functions for Simulation of Cloud and Dusty Surfaces*, Computer Graphics, 16:3, pp. 21-29.

CIE-110-1994 (1994). *Spatial distribution of daylight - luminance distributions of various reference skies*, Tech. rep., International Commission on Illumination.

Considine D.M., ed. (1976). *Van Nostrand's Scientific Encyclopedia*, Van Nostrand Reinhold Company, New York

Ferwerda J. A., Pattanaik S., Shirley P., Greenberg D. P. (1996). *A Model of Visual Adaptation for Realistic Image Synthesis*. In SIGGRAPH 96 Conference Proceedings, pages 249–258.

Fournier A. (1989). *The Modelling of Natural Phenomena*, Proceedings of the Graphics Interface '89 - Vision Interface '89, Toronto, Ontario, Canadian Information Processing Society.

Grace A. (1992). *Optimization Toolbox- For use with Matlab*, The Math Works Inc., Natick.

Gueymard, C.. (1995). *A Simple Model of the Atmospheric Radiative Transfer of Sunshine: Algorithm and Performance Assessment*. FSEC-PF-270-95.

Haltrin V. (1996). *A real-time algorithm for atmospheric corrections of airborne remote optical measurements above the ocean*. In Proceedings of the Second International Airborne Remote Sensing Conference and Exhibition, volume III, pages 63–72. Environmental Research Institute of Michigan.

Henyey. L.G., and Greenstein, J.L. (1941). *Diffuse reflection in the Galaxy*. Astrophysical Journal 93:70

Hoffman N. and Preetham A.J. (2002). *Rendering Outdoor Light Scattering in Real Time*. In Proceedings of the Game Developer Conference. Game Developers Conference.

Ineichen P., Molineaux B. and Perez R (1994). *Sky luminance data validation: comparison of seven models with four data banks*. *Solar Energy 52*, 4, 337–346.

Iqbal M. (1983). *An Introduction to Solar Radiation.* Academic Press, Toronto.

Johnson G. and Fairchild M. (1999). *Full-spectral color calculations in realistic image synthesis*. IEEE Computer Graphics and Applications, 19(4):47-53, July/August 1999.

Kaneda K., Okamoto T., Nakamae E., and Nishita T. (1991). *Photorealistic Image Synthesis for Outdoor Scenery Under Various Atmospheric Conditions*. Visual Computer, 7(5): 247–258.

Klassen R. V. (1987). *Modeling the Effect of the Atmosphere on Light*. ACM Transactions on Graphics, 6(3): 215–237.

Larson G. W. and Rushmeier H., Piatko C. (1997). *A Visibility Matching Tone Reproduction Operator for High Dynamic Range Scenes*. IEEE Transactions On Visualization and Computer Graphics, 3(4): 291–306.

Levenberg K. (1944). *A Method for the Solution of Certain Problems in Least Squares*. Quart. Appl. Math. Vol. 2, pages 164-168.

Marquardt D. (1963). *An Algorithm for Least-Squares Estimation of Nonlinear Parameters*. SIAM J. Appl. Math. Vol. 11, pages 431-441

McCartney E. J. (1976). *Optics in the atmosphere*, Wiley, New York

McKenna D., Avila R., J. Hill M., Hippler S., Salinari P., Stanton P., Weiss R.. (2003), *The LBT Facility SCIDAR: Recent Results.* Adaptive Optics System Technologies II, P. Wizinowich and D. Bonaccini eds., Hawaii EUA, SPIE Proc. 4839, 825-836.

Miller. (1982), *Lockheed's Skunk Works: The First Fifty Years*. Arlington, Texas: Aerofax, Inc.

Minnaert M. (1954). *The Nature of Light and Color in the Open Air*, Dover.

Musgrave F.K. (1993). *Methods for Realistic Landscape Imaging*, Yale University Department of Computer Science, TR-1038.

Nielsen, R. S. (2003). *Real Time Rendering of Atmospheric Scattering Effects for Flight Simulators*, Informatics and Mathematical Modelling, Technical University of Denmark, DTU

Nishita, T., Dobashi, Y., Kaneda, K., and Yamashita, H. (1996). *Display method of the sky color taking into account multiple scattering*. In Pacific Graphics, pp. 117-132,.

Oreskes N., Shrader-Frechette K. and Belitz K. (1994). *Verification, validation, and confirmation of numerical models in the earth sciences*. Science 263:641-646.

Perez R., Seals R., and Michalsky J..(1993). *All-Weather Model for Sky Luminance Distribution - Preliminary Configuration and Validation.*

Poynton C. A. (1995). *A guided tour of color space*, in: SMPTE Advanced Television and Electronic Imaging Conf., San Fransisco, 167-180.

Preetham A. J., Shirley P., and Smits B.. (1999). *A Practical Analytic Model for Daylight*. In Proceedings of the 26th Annual Conference on Computer Graphics and Interactive Techniques, pages 91–100. ACM Press/Addison-Wesley Publishing Co.

Preetham A. J. (2003). *Modelling Skylight and Aerial Perspective: SIGGRAPH Course Note*. SIGGRAPH.

Rayleigh, L. (1871). *On the scattering of light by small particles*. Philosophical Magazine 41, 447-451

Tumblin J. and Rushmeier H. (1993). *Tone Reproduction for Realistic Images*. IEEE Computer Graphics and Applications, 13(6): 42–48.

Lampiran 20
UTM/RMC/F/0024 (1998)

UNIVERSITI TEKNOLOGI MALAYSIA

BORANG PENGESAHAN
LAPORAN AKHIR PENYELIDIKAN

TAJUK PROJEK : The Development of Local Solar Irradiance for Outdoor Computer Graphics Rendering

Saya : **DR** ISMAIL BIN MAT AMIN
(HURUF BESAR)

Mengaku membenarkan Laporan Akhir Penyelidikan ini disimpan di Perpustakaan Universiti Teknologi Malaysia dengan syarat-syarat kegunaan seperti berikut :

1. Laporan Akhir Penyelidikan ini adalah hakmilik Universiti Teknologi Malaysia
2. Perpustakaan Universiti Teknologi Malaysia dibenarkan membuat salinan untuk tujuan rujukan sahaja.
3. Perpustakaan dibenarkan membuat penjualan salinan Laporan Akhir Penyelidikan ini bagi kategori TIDAK TERHAD
4. * Sila tandakan (/)

☐	SULIT	(Mengandungi maklumat yang berdarjah keselamatan atau Kepentingan Malaysia seperti yang termaktub di dalam AKTA RAHSIA RASMI 1972)
☐	TERHAD	(Mengandungi maklumat TERHAD yang telah ditentukan oleh Organisasi/badan di mana penyelidikan dijalankan)
☐	TIDAK TERHAD	

_____
TANDATANGAN KETUA PENYELIDIK

_____
Nama & Cop Ketua Penyelidik

Tarikh : _____

LAPORAN PENYELIDIKAN

DEVELOPMENT OF AN EFFICIENT CURSIVE HANDWRITING RECOGNITION SYSTEM USING HYBRID INTELLIGENT TECHNIQUES

VOT RMC 74136

PENYELIDIK:

DR. DZULKIFLI MOHAMAD

DR. SITI MARIYAM HJ. SHAMSUDDIN

MUHAMMAD FAISAL ZAFAR

PUSAT PENGURUSAN PENYELIDIKAN

UNIVERSITI TEKNOLOGI MALAYSIA

SESI 2003 / 2005

DEVELOPMENT OF AN EFFICIENT CURSIVE HANDWRITING RECOGNITION SYSTEM USING HYBRID INTELLIGENT TECHNIQUES

IRPA 2003 / 2005

KETUA PENYELIDIK:

DR. DZULKIFLI MOHAMAD (JAN 2003 – JUNE 2005)

PENYELIDIK:

DR. DZULKIFLI MOHAMAD
DR. SITI MARIYAM HJ. SHAMSUDDIN
MUHAMMAD FAISAL ZAFAR

Faculty of Computer Science and Information System
Universiti Teknologi Malaysia
Skudai, Johor.

TEMPOH PENYELIDIKAN: JANUARY 2003 – JUNE 2005
VOT RMC 74136

PUSAT PENGURUSAN PENYELIDIKAN
UNIVERSITI TEKNOLOGI MALAYSIA

R & D DIRECTORY UTM

VOT:	74136
PROJECT TITLE:	DEVELOPMENT OF AN EFFICIENT CURSIVE HANDWRITING RECOGNITION SYSTEM USING HYBRID INTELLIGENT TECHNIQUES
HEAD OF RESEARCHERS:	DR. DZULKIFLI MOHAMAD (JAN 2003 – JUNE 2005)
RESEARCHERS:	DR. SITI MARIYAM HJ. SHAMSUDDIN MUHAMMAD FAISAL ZAFAR
FACULTY:	FACULTY OF COMPUTER SCIENCE AND INFORMATION SYSTEM UNIVERSITI TEKNOLOGI MALAYSIA SKUDAI, JOHOR.
KEYWORDS:	CURSIVE HANDWRITTEN WORD RECOGNITION, HOLISTIC APPROACH, FEATURE SELECTION/EXTRACTION, CHARACTER/WORD CLASSIFICATION
DATE OF COMPLETION:	JUNE 2005

Lampiran 20
UTM/RMC/F/0024 (1998)

UNIVERSITI TEKNOLOGI MALAYSIA

BORANG PENGESAHAN
LAPORAN AKHIR PENYELIDIKAN

TAJUK PROJEK : The Development of Local Solar Irradiance for Outdoor Computer Graphics Rendering

Saya : **DR** ISMAIL BIN MAT AMIN
(HURUF BESAR)

Mengaku membenarkan Laporan Akhir Penyelidikan ini disimpan di Perpustakaan Universiti Teknologi Malaysia dengan syarat-syarat kegunaan seperti berikut :

1. Laporan Akhir Penyelidikan ini adalah hakmilik Universiti Teknologi Malaysia
2. Perpustakaan Universiti Teknologi Malaysia dibenarkan membuat salinan untuk tujuan rujukan sahaja.
3. Perpustakaan dibenarkan membuat penjualan salinan Laporan Akhir Penyelidikan ini bagi kategori TIDAK TERHAD
4. * Sila tandakan (/)

☐	SULIT	(Mengandungi maklumat yang berdarjah keselamatan atau Kepentingan Malaysia seperti yang termaktub di dalam AKTA RAHSIA RASMI 1972)
☐	TERHAD	(Mengandungi maklumat TERHAD yang telah ditentukan oleh Organisasi/badan di mana penyelidikan dijalankan)
☐	TIDAK TERHAD	

_____
TANDATANGAN KETUA PENYELIDIK

_____
Nama & Cop Ketua Penyelidik

Tarikh : _____

TABLE OF CONTENTS

Solar Attenuation Due to Absorption and Scattering Processes

Irwandi Hipni Mohamad Hipiny[1] Ismail Mat Amin[2] Noor Azam Md. Sheriff[3]
Computer Graphics and Multimedia Department,
Faculty of Computer Science and Information System
Universiti Teknologi Malaysia
81310 Johor, Malaysia
[1]*irwandi@itc.utm.my* [2]*ismail@fsksm.utm.my* [3]*azam@fsksm.utm.my*

Abstract

Sky color depends greatly on the contents of the local atmosphere. This layer of ozone, mixed gases, (CO, CO_2, O_2, N_2, CH_4 and NO_2) and water vapor causes absorption to the radiation emanated from the sun while molecules and aerosols scatters the radiation randomly. Both processes will cause the solar radiance to be attenuated thus resulting a lower energy value when they finally reach the earth surface. It is important for us to be able to predict correctly the resulting accumulated irradiance value as this quantity is important for various usages in engineering and biological applications such as building architectural design, vegetation and et cetera. In order to do the prediction correctly, we need a model which can closely and accurately resemble the real thing. This paper aim to provide the readers an insightful peek at the theory behind both scattering and absorption processes plus the existing formulation used to calculate attenuation coefficients for each processes components. This knowledge will be vital as a basis for determining our very own localized attenuation coefficient/monochromatic extinction model or helping us understand the existing ones better.

1. Introduction

Our earth's atmosphere is shaped as a hemispherical dome; consisting a mixture of air molecules, aerosols and other small particles which vary exponentially with the altitude. The presence of these elements helps create the visually rich appearances of the sky by affecting the sunlight entering our atmosphere via absorption and scattering process. Where and in what order this attenuation take place does not matter because attenuation is multiplicative thus commutative [2]. Minnaert [3] described these processes in detail in his classic book and has been further discussed by Lynch and Livingston [4] with several further extensions.

There has been a lot of interest regarding solar attenuation in computer graphic research community. Models of atmospheric particles behaviors in the atmosphere between light sources (sun) and the objects are in demand as the need for more realistic rendered sky increase by day. The sun's extraterrestrial spectral radiance is multiplied with the spectral attenuation/total attenuation coefficient due to each atmospheric constituent which respond to either scattering or absorption behavior in order to calculate the sun's spectral radiance arriving at earth's surface. This solar depletion can be quantified by the monochromatic extinction coefficient,

$$\tau_\lambda = \exp\left[k_{r\lambda} + k_{\alpha\lambda}m_\alpha + k_{o\lambda}m_o + k_{g\lambda}m_g + k_{w\lambda}m_w + k_{n\lambda}m_n\right]$$

Where the indices r, α, o, g, w and n refer to Rayleigh and Mie scattering and to absorption due to ozone, mixed gases, water vapor and NO_2.

2. Scattering

The earth atmosphere receives almost parallel illumination from the sun. This light will then undergo scattering process due to the presence of air molecules and aerosols in the air. Light may scatter several times but the primary scattering will be only taken into account as it is far more dominant compared to secondary, tertiary and the rest. Single scattering is sufficient as the albedo of the atmosphere is relatively low. Previous approaches make use of single scattering but the usage of multiple scattering has gain popularity as today hardware technology are more than capable of handling such complex calculation. Nishita (5) introduced

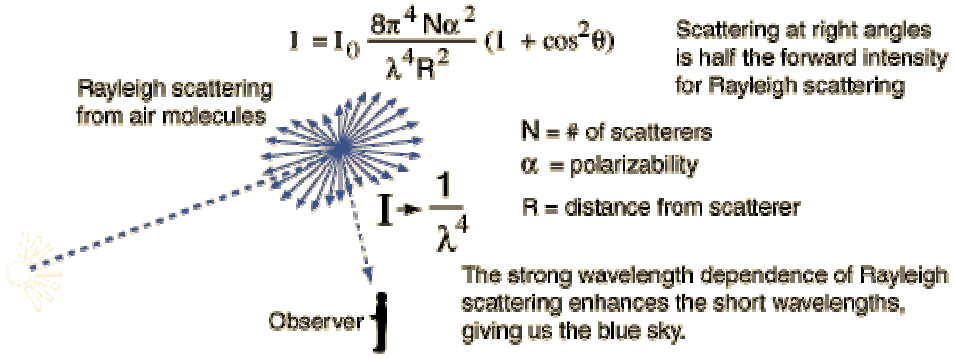

Figure 1. Rayleigh scattering

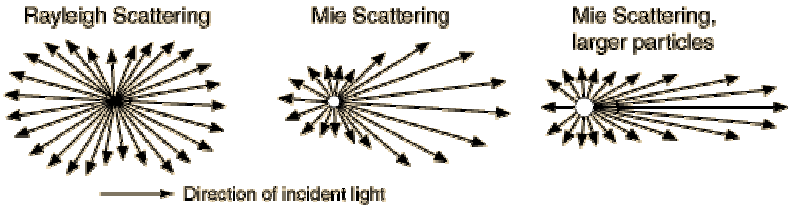

Figure 2. Mie scattering

look-up table approach which is made using the geometric properties of the atmosphere around the earth in order to speed up the sky color calculation which takes multiple scattering into account. The scattering from molecules and very tiny particles (<1/10 wavelength) is predominantly Rayleigh scattering while for particle with size larger than a wavelength, Mie scattering predominates.

2.1 Rayleigh scattering

Rayleigh scattering (Fig.1) explains the scattering due to particles smaller than a wavelength (air molecules). It can be considered as elastic scattering since the photon energies of the scattered photons remains unchanged. Rayleigh scattering assumes that all scattering particles are spherical and that they scatter independently of one another. It also strongly favors short wavelengths thus producing colors near the blue end of the color spectrum. Leckner (6) devised an approximate formula for $k_{r\lambda}$:

$$k_{r\lambda} = 0.008735\lambda^{-4.08}$$

m_r was given by Gueymard (7) as,

$$m_r = \left[\cos z + 1.76759 \times 10^{-3} z(94.37515 - z)^{-1.21563}\right]^{-1}$$

2.2 Mie scattering

Mie scattering (Fig.2) explains the scattering due to particles larger than a wavelength (aerosols). It produces a pattern like an antenna lobe, with a sharper and more intense forward lobe for larger particles. Mie scattering is not strongly wavelength dependent thus producing white lights.

Ångström (8, 9) proposed his single turbidity formula for the extinction coefficient of the aerosols as,

$$k_{\alpha\lambda} = \beta\lambda^{-\alpha}$$

where β is called Ångström's turbidity coefficient with values varying in the range 0-0.5, and α is the wavelength exponent with a value typically in the range of 0.5-2.5. The commonly used value for α is 1.3.

Gueymard (7) presents m_α as,

$$m_\alpha = \left[\cos z + 4.29452 \times 10^{-4} z(92.24849 - z)^{-1.2529}\right]^{-1}$$

McClatchey and Selby (10) have produced with a simple model for β:

$$3.912/vis - \beta = 0.55^{\alpha}(0.01162)[0.024729(vis-5)+1.132]$$

where *vis* is the visibility in the horizontal direction (km). This value is dependence to the atmospheric conditions. A cleaner condition will give a higher *vis* value compared to a very turbid atmosphere. Iqbal (11) listed the *vis* values for each four atmospheric conditions namely clean, clear, turbid and very turbid.

3.0 Absorption

The absorption of radiation is due to ozone, mixed gases and water vapors. The incoming radiant flux converts a part of its incident energy into another form such as photochemical processes and absorbed by the matter.

3.1 Absorption by Ozone

Absorption by ozone differs within wavelength. It absorbs weakly in the near infrared, moderately in the visible band and strongest in the ultraviolet waveband. Temperature-wise, $k_{o\lambda}$ is obtained using formulation below suggested by Smith et al. (12):

$$k_{o\lambda}(T_{eo}) = \max\left[0, k_{o\lambda}(T_{ro}) + C_1(T_{eo}-T_{ro}) + C_2(T_{eo}-T_{ro})^2\right]$$

Further explanation on this formulation can be obtained in (1).

According to Gueymard (7),

$$m_o = \left[\cos z + 1.07489\times10^{-2} z(96.62667 - z)^{-1.3882}\right]^{-1}$$

3.2 Absorption by Mixed Gases

Mixed gases (O_2 and CO_2) concentration decrease monotonically according to latitude. We can obtained $k_{g\lambda}$ using Pierluissi and Tsai (13, 14) mixed gas transmittance formulation $\tau_{g\lambda}$,

$$\tau_{g\lambda} = \exp\left[-\left(k_{g\lambda} l_g m_g\right)^C\right]$$

According to Gueymard (7),

$$m_g = \left[\cos z + 1.76759\times10^{-3} z(94.37515 - z)^{-1.21563}\right]^{-1}$$

Further explanation on this formulation can be obtained in (1).

3.3 Absorption by Water Vapor

We can obtained $k_{w\lambda}$ using Pierluissi et al. (15) water vapor transmittance formulation $\tau_{w\lambda}$,

$$\tau_{w\lambda} = \exp-\left[\left(k_{w\lambda}\left(m_w l_w\right)^{1.05} f_w^n B_w\right)^C\right]$$

According to Gueymard (7),

$$m_w = \left[\cos z + 4.29452\times10^{-4} z(92.24849 - z)^{-1.2529}\right]^{-1}$$

Further explanation on this formulation can be obtained in (1).

4.0 Conclusion

Both scattering and absorption play major role is solar attenuation process. Both affect the incoming solar radiation in different ways thus both cases should be handle differently. There have been a lot of research studies devoted to this particular area and still, there is a lot left to be desired. We need a better, faster, more precise model to obtain higher quality result. Even more, the above formulations are tailor-made for European skies thus bringing in opportunity for us to develop our very own local model. Tropical countries such as Malaysia has our very own unique atmosphere which differs greatly compared to skies at the other part of the world. By developing our very own model to predict this work of nature, we will obtain a better and more precise irradiance values prediction; tailor-made for our very own country needs.

References

[1] Muneer, T., "Solar Radiation & Daylight Models for the Energy Efficient Design of Buildings", Architectural Press, 1997.

[2] A. J. Preetham, Peter Shirley, Brian Smits, "A Practical Analytic Model for Daylight", Proceedings of The 26th Annual Conference on Computer Graphics and Interactive Techniques, pp.91-100, July 1999.

[3] Minnaert, M., “Light and Color in the Open Air”, Dover, 1954.

[4] Lynch, D.K., & Livingston, W. “Color and Light in Nature”, Cambridge University Press, 1995.

[5] Nishita, T., Dobashi, Y., Kaneda, K., Yamashita, H., "Display Method of the Sky Color Taking Into Account Multiple Scattering", Pacific Graphics'96, pp.117-132, 1996.

[6] Leckner, B. "The Spectral Distribution of Solar Radiation at the Earth’s Surface: Elements of a Model", Solar Energy, 20, 143, 1978.

[7] Gueymard, C. "Simple Model of the Atmospheric Radiative Transfer of Sunshine (SMARTS2): Algorithms and Performance Assessment", FSEC-PF-270-94, Florida Solar Energy Center, Cocoa, FL, 1994.

[8] Ångström, A. "On the Atmospheric Transmission of Sun Radiation and on Dust in the Air", Geografis.Annal.2, 155, 1929.

[9] Ångström, A. "On the Atmospheric Transmission of Sun Radiation", Geograf.Annal.2, 130, 1929.

[10] McClatchey, R.A & Selby, J.E. "Atmospheric Transmittance from 0.25 to 38.5 μm: Computer Code LOWTRAN2”, AFCRL-72-0745, Environ. Res. Paper 427, 1972.

[11] Iqbal, M., “An Introduction to Solar Radiation”, Academic Press, Toronto, 1983.

[12] Smith, E.U.P., Wan, Z. & Baker, K.S, “Ozone Depletion in Antarctica: Modeling its Effect on Solar UV Irradiance under Clear-Sky Conditions”, J. Geoph. Res97C, 7383, 1992.

[13] Pierluissi, J.H., & Tsai, C.M, “Molecular Transmittance Band Model for Oxygen in the Visible”, Appl. Opt. 25, 2458, 1986.

[14] Pierluissi, J.H., & Tsai, C.M, “New LOWTRAN Models for the Uniformly Mixed Gases”, Appl. Opt. 26, 616, 1987.

[15] Pierluissi, J.H., & Maragoudakis, C.E & Tehrani-Morahed, R. “New LOWTRAN Models for Water Vapor”, Appl. Opt. 28, 3792,1989

BENEFIT REPORT

I. Description of the Project

A. Project Identification

1. Project number : 74135
2. Project title : The Development of Local Solar Irradiance for Outdoor Computer Graphics Rendering
3. Project Leader : Ismail Mat Amin

B. Type of research

Indicate the type of research of the project *(Please see definitions in the Guidelines for completing the Application Form)*

	Scientific research (fundamental research)
√	Technology development (applied research)
	Product/process development (design and engineering)
	Social/policy research

C. Objectives of the project

1. Socio-economic objectives

   Which socio-economic objectives are addressed by the project? *(Please identify the sector, SEO Category and SEO Group under which the project falls. Refer the Malaysian R&D Classification System brochure for SEO Group code)*

   Sector : **Services and IT**

   SEO Category : **Computer Software and Services (S20900)**

   SEO Group and Code : **S20999 (Other Information and Communication Services Not Elsewhere Defined)**

2. Fields of research

   Which are the two main FOR Categories, FOR Group, and FOR Areas of your project? *(Please refer to the Malaysia R&D Classification System brochure for the FOR Group Code)*

   a. Primary field of research

      FOR Category : **Information & Communication Technologies**

      FOR Group and Code : Information System (F10501)

      FOR Area : Computer Graphics

b. Secondary field of research

FOR Category: **F10500 Information, Computer and Communication Technologies**

FOR Group and Code: **Software (F10503)**

FOR Area: Other Software

D. Project duration

What was the duration of the project?

24 Months + 6 months extension

E. Project manpower

How many man-months did the project involve?

76 man-months

F. Project costs

What were the total project expenses of the project

RM 139,278.98

G. Project funding

Which were the funding sources for the project?

Funding sources	**Total Allocation (RM)**
IRPA	RM 183,160.00
_____	_____

II. Direct Output of the Project

A. Technical contribution of the project

1. What was the achieved direct output of the project:

For scientific (fundamental) research projects?

- [√] Algorithm
- [ ] Structure
- [ ] Data
- [ ] Other, Please specify:

_____

For technology development (applied research) project:

- [ ] Method/technique
- [√] Demonstrator/prototype
- [ ] Other, Please specify:

_____

For product/process development (design and engineering) projects:

- [ ] Product/component
- [ ] Process
- [√] Software
- [ ] Other, Please specify:

_____

2. How would you characterize the quality of this output?

- [ ] Significant breakthrough
- [√] Major improvement
- [ ] Minor improvement

B. Contribution of the project knowledge

1. How has the output of the project been documented?

- [√] Detailed project report
- [ ] Product/process specification documents
- [ ] Other, please specify:

_____

2. Did the project create an intellectual property stock?

- [ ] Patent obtained
- [ ] Patent pending
- [ ] Patent application will be filed
- [ ] Copyright

3. What publications are available?

- [ ] Articles (s) in scientific publications How many:
- [√] Papers (s) delivered at conferences/seminars How many: 2
- [ ] Book
- [ ] Other, Please specify:

Thesis 1, Papers 2

4. How significant are citations of the results?

- [ ] Citations in national publications How many:
- [ ] Citations in international publications How many:
- [ ] Not Yet
- [√] Not known

III. Organizational Outcomes of the Project

A. Contribution of the project to expertise development

1. How did the project contribute to expertise?

- [ ] PhD degrees — How many:
- [√] MSc degrees — How many: 1
- [ ] Research staff with new specialty — How many:
- [ ] Other, Please specify: _____

2. How significant is this expertise?

- [ ] One of the key areas of priority for Malaysia
- [√] An important area, but not a priority one

B. Economic contribution of the project?

1. How has the economic contribution of the project materialized?

- [ ] Sales of manufactured product/equipment
- [ ] Royalties from licensing
- [ ] Cost saving
- [√] Time saving
- [ ] Other, Please specify: _____

2. How important is this economic contribution?

- [ ] High economic contribution — Value : RM
- [ ] Medium economic contribution — Value : RM
- [√] Low economic contribution — Value : RM

3. How important is this economic contribution?

- [ ] Already materialized
- [ ] Within months of project completion
- [ ] Within three years of project completion
- [ ] Expected in three of project completion
- [√] Unknown

C. Infrastructural contribution of the project

1. What infrastructural contribution has the project had?

- [ ] New equipment — Value : RM
- [ ] New/improved facility — Investment : RM
- [ ] New information networks
- [√] Other, Please specify:
  Atmospheric profile model

2. How significant is this infrastructural contribution for the organization?

- [ ] Not significant/does not leverage other projects
- [√] Moderately significant
- [ ] Very significant/significantly leverages other projects

D. Contribution of the project to the organization's reputation

1. How has the project contributed to increasing the reputation of the organization

- [ ] Recognition as a Centre of Excellence
- [ ] National award
- [ ] International award
- [√] Demand for advisory services
- [ ] Invitations to give speeches on conferences
- [ ] Visits from other organization
- [ ] Other, Please specify:
  _____

2. How important is the project's contribution to the organization's reputation?

- [ ] Not significant
- [√] Moderately significant
- [ ] Very significant

IV. National Impacts of the Project

A. Contribution of the project to organizational linkages

1. Which kinds of linkages did the project create?

- [√] Domestic industry linkages
- [ ] International industry linkages
- [ ] Linkages with domestic research institutions, universities
- [√] Linkages with international research institutions, universities

2. What is the nature of the linkages

- [ ] Staff exchanges
- [ ] Inter-organizational project team
- [ ] Research contract with a commercial client
- [√] Informal consultation
- [ ] Other, Please specify:

B. Social-economic contribution of the project

1. Who are the direct customer/beneficiaries of the project output?

Customers/beneficiaries:	**Number:**
•	

2. Who has/will the socio-economic contribution of the project materialized?

- [ ] Improvements in health
- [ ] Improvements in safety
- [ ] Improvements in the environment
- [ ] Improvements in the energy consumption
- [ ] Improvements in the international relations
- [√] Other, Please specify:

Improve in provision of meteorological profiling

3. How important is this socio-economic contribution?

- [ ] High social contribution
- [√] Medium social contribution
- [ ] Low social contribution

4. When has/will this social contribution materialized?

- [ ] Already materialized
- [ ] Within three years of project completion
- [ ] Expected in three years or more
- [√] Unknown

Date: **Signature:**

LAPORAN PENYELIDIKAN

THE DEVELOPMENT OF LOACAL SOLAR IRRADIANC E MODEL FOR OUTDOOR COMPUTER GRAPHICS RENDERING

VOT RMC 74135

PENYELIDIK:

DR. ISMAIL MAT AMIN

PROF. DR. GHAZALI SULONG

PROF. MADYA DR. IBRAHIM BUSU

PROF. MADYA SARUDIN KARI

PROF. MADYA DAUT BIN DAMAN

MOHD SHAHRIZAL SUNAR

PUSAT PENGURUSAN PENYELIDIKAN

UNIVERSITI TEKNOLOGI MALAYSIA

SESI 2003 / 2005

THE DEVELOPMENT OF LOCAL SOLAR IRRADIANCE MODEL FOR OUTDOOR COMPUTER GRAPHICS RENDERING

IRPA 2003 / 2005

KETUA PENYELIDIK:

DR ISMAIL MAT AMIN (JANUARI 2003 – JUN 2005)

PENYELIDIK:

DR. ISMAIL MAT AMIN

PROF. DR. GHAZALI SULONG

PROF. MADYA DR. IBRAHIM BUSU

PROF. MADYA SARUDIN KARI

PROF. MADYA DAUT BIN DAMAN

MOHD SHAHRIZAL SUNAR

Faculty of Computer Science and Information System

Universiti Teknologi Malaysia

Skudai, Johor.

TEMPOH PENYELIDIKAN: JANUARI 2003 – JUN 2005

VOT RMC 74135

PUSAT PENGURUSAN PENYELIDIKAN

UNIVERSITI TEKNOLOGI MALAYSIA

R & D DIRECTORY UTM

VOT:	74135
PROJECT TITLE:	THE DEVELOPMENT OF LOCAL SOLAR IRRADIANCE FOR OUTDOOR COMPUTER GRAPHICS RENDERING
HEAD OF RESEARCHERS:	DR. ISMAILMAT AMIN (JANUARI 2003 – JUN 2005)
RESEARCHERS:	DR. ISMAIL MAT AMIN PROF. DR. GHAZALI SULONG PROF. MADYA DR. IBRAHIM BUSU PROF. MADYA SARUDIN KARI PROF. MADYA DAUT BIN DAMAN MOHD SHAHRIZAL SUNAR
FACULTY:	FACULTY OF COMPUTER SCIENCE AND INFORMATION SYSTEM UNIVERSITI TEKNOLOGI MALAYSIA SKUDAI, JOHOR.
KEYWORDS:	COMPUTER GRAPHICS ATMOSPHERIC MODEL NUMERICAL MODELLING SOLAR RADIATION IMAGE SYNTHESIS
DATE OF COMPLETION:	JUN 2005

End of Project Report Guidelines

A. Purpose

The purpose of the End of Project is to allow the IRPA Panels and their supporting group of experts to assess the results of research projects and the technology transfer actions to be taken.

B. Information Required

The following Information is required in the End of Project Report :

- Project summary for the Annual MPKSN Report;
- Extent of achievement of the original project objectives;
- Technology transfer and commercialization approach;
- Benefits of the project, particularly project outputs and organisational outcomes; and
- Assessment of the project team, research approach, project schedule and project costs.

C. Responsibility

The End of Project Report should be completed by the Project Leader of the IRPA-funded project.

D. Timing

The End of Project Report should be submitted within three months of the completion of the research project.

E. Submission Procedure

One copy of the End of Project is to be mailed to :

IRPA Secretariat
Ministry of Science, Technology and the Environment
14th Floor, Wisma Sime Darby
Jalan Raja Laut
55662 Kuala Lumpur

End of Project Report

A. Project number : 74135

Project title : The Development of Local Solar Irradiance for Outdoor Computer Graphics Rendering.

Project leader: Ismail Mat Amin

Tel: 07 5532345 **Fax:** 07 556 5044

B. Summary for the MPKSN Report (for publication in the Annual MPKSN Report, please summarise the project objectives, significant results achieved, research approach and team strucure)

Objectives:

1. To develop a numerical solar radiation model for Malaysian environment.
2. To investigate, analyse and formulate the solar radiation model into computer graphics rendering.
3. To develop a solar radiation computer based simulator for outdoor scene.

Achievements:

1. Local atmopheric profile characterisation
2. Simple outdoor real-time sky rendering

Approach:

1. Testing global models and data collection procedures
2. Data processing and model verification
3. Computer simulation of the regional model for solar radiation
4. Production of a regional solar irradiance map
5. Applications and the presentation of Final Product

C. Objectives achievement

- **Original project objectives** (Please state the specific project objectives as described in Section ll of the Application Form)

a) To develop a numerical solar radiation model for Malaysian environment.
b) To investigate, analyse and formulate the solar radiation model into computer graphics rendering.
c) To develop a solar radiation computer based simulator for outdoor

- **Objectives Achieved** (Please state the extent to which the project objectives were achieved)

All objectives are achived as planned.

- **Objectives not achieved** (Please identify the objectives that were not achieved and give reasons)

D. Technology Transfer/Commercialisation Approach (Please describe the approach planned to transfer/commercialise the results of the project)

a) Technical paper
    a. A survey of colour computation methods of the sky, in proceedings of international symposium and exhibition on geoinformation, ISG 2004
    b. Daylight sky rendering for flight simulators (preliminary results), in proceeding of PARS 2005

b) Reports – A detailed report has been documented in order to assist the user in using the developed system.

E. Benefits of the Project (Please identify the actual benefits arising from the project as defined in Section lll of the Application Form. For examples of outputs, organisational outcomes and sectoral/national impacts, please refer to Section lll of the Guidelines for the Application of R&D Funding under IRPA)

- **Outputs of the project and potential beneficiaries** (Please describe as specifically as possible the outputs achieved and provide an assessment of their significance to users)

The projects have created data profiles and modules/libraries routines that can be used in generating or creating the sky colour rendering for outdoor scenes.

The real benefit of these routines is that they can be used in applications such as flight simulators or other real-time computer graphics rendering.

The benefits will be to the organizations such as:

1) Governmental sectors (Meteorological services)
2) Private Sectors (Game development and interactive simulations)
3) Universities & Colleges
4) Researchers

- **Organisational Outcomes** (Please describe as specifically as possible the organisational benefits arising from the project and provide an assessment of their significance)

Post-graduate student (1 Msc)
Atmospheric data processing and profiling
Simple sky color generator for flight simulators

Research Linkages
The faculty has been recognised by the Meteorological Services to be the premier computer graphics research center with emphasis to real-time atmospheric rendering and simulations.

Consultations
Informal discussion with private bodies and Malaysian Navy on the development of gun trainer and simulators.

- **National Impacts** (If known at this point in time, please describes specifically as possible the potential sectoral/national benefits arising from the project and provide an assessment of their significance)

1. Domestic industry linkages – This project able to establish link between any of government agencies in Malaysia and Faculty of Computer Science and Information Systems, UTM..

2. Cost – All agencies in Malaysia can use local software product.

3. Computer Developers – can used the libraries/routines to develop other products.

F. Assessment of project structure

- **Project Team** (Please provide an assessment of how the project team performed and highlight any significant departures from plan in either structure or actual man-days utilized)

The team work objectively towards the success of the projects. Formal and informal discussions about the project progress were made every two-weeks. The progress and constrains of the project has to be revised extensively due to the fact that the field data acquisitions were rather tedious and time consuming. Additionally this problem is compounded during the model development as there is no prior works to be referred to. Consequently, a six months extension was requested in order to conclude the project successfully.

- **Collaborations** (Please describe the nature of collaborations with other research organizations and/or industry)

G. Assessment of Research Approach (Please highlight the main steps actually performed and indicate any major departure from the planned approach or any major difficulty encountered)

All the phases of the project development, namely

1. Testing global models and data collection procedures
2. Data processing and model verification
3. Computer simulation of the regional model for solar radiation
4. Production of a regional solar irradiance map
5. Applications and the presentation of Final Product

Have been achieved as mentioned above with minor variances.

H. Assessment of the Project Schedule (Please make any relevant comment regarding the actual duration of the project and highlight any significant variation from plan)

The project has been successfully completed with a six month extension due to the aforementioned constraints. The six months extension allows us to refine and fine-tune our methodology so as to fall inline with the research design.

I. Assessment of Project Costs (Please comment on the appropriateness of the original budget and highlight any major departure from the planned budget)

A few equipments cannot be acquired due to financial disbursements problems. This technical hitch forces us to rely on semi-automatic methods to acquire and process out data.

J. Additional Project Funding Obtained (In case of involvement of other funding sources, please indicate the source and total funding provided)

K. Other Remarks (Please include any other comment which you feel is relevant for the evaluation of this project)

Date : **Signature :**

UNIVERSITI TEKNOLOGI MALAYSIA
Research Management Centre

PRELIMINARY IP SCREENING & TECHNOLOGY ASSESSMENT FORM

(To be completed by Project Leader submission of Final Report to RMC or whenever IP protection arrangement is required)

1. **PROJECT TITLE IDENTIFICATION** : The Development of Local Solar Irradiance for Outdoor Computer Graphics Rendering

._____ Vote No: 74135

2. **PROJECT LEADER** :

Name : Ismail bin Mat Amin

Address : _____FSKSM, UTM 8130 Johor _____

Tel : ___07 5532345___ Fax : ____07 55 65044____ e-mail : _ismailma@utm.my _

3. **DIRECT OUTPUT OF PROJECT** *(Please tick where applicable)*

Secientific Research	Applied Research	Product/Process Development
☑ Algorithm	☐ Method/Technique	☐ Product / Component
☐ Structure	☑ Demonstration / Prototype	☐ Process
☐ Data		☑ Software
☐ Other, please specify	☐ Other, please specify	☐ Other, please specify
_____	_____	_____
_____	_____	_____
_____	_____	_____

4. INTELLECTUAL PROPERTY *(Please tick where applicable)*

☑ Not patentable	☐ Technology protected by patents
☐ Patent search required	☐ Patent pending
☐ Patent search completed and clean	☐ Monograph available
☐ Invention remains confidential	☐ Inventor technology champion
No publications pending	☐ Inventor team player
☐ No prior claims to the technology	☐ Industrial partner identified

5. LIST OF EQUIPMENT BOUGHT USING THIS VOT

2 Laptops with upgraded facilities

1 Desktop Computer

1 Laser Printer

6. STATEMENT OF ACCOUNT

a)	APPROVED FUNDING	RM : 183,160.00
b)	TOTAL SPENDING	RM : 139,278.98
c)	BALANCE	RM : 43,881.02

7. TECHNICAL DESCRIPTION AND PERSPECTIVE

Please tick an executive summary of the new technology product, process, etc., describing how it works. Include brief analysis that compares it with competitive technology and signals the one that it may replace. Identify potential technology user group and the strategic means for exploitation.

a) Technology Description

The algorithm developed were based upon the SMARTS-2 solar energy irradiance program. An extensive modifications and extensions were developed in order to make the base program capable of rendering sky colour in real-time.

b) Market Potential

At the moment, no market study and requirement has been made to determine the marketablility of the research results and algorithms. In spite of this setback, the suitability of the algorithms with the respective atmospheric profile in real-time simulation cannot be denied.

c) Commercialisation Strategies

Unfortunely, this item is not emphasized due to the fact that it is outside the scope of study.

Signature of Projet Leader :- Date :-

_____ _____

8. RESEARCH PERFORMANCE EVALUATION

a) FACULTY RESEARCH COORDINATOR

Research Status	( )	( )	( )	( )	( )	( )
Spending	( )	( )	( )	( )	( )	( )
Overall Status	( )	( )	( )	( )	( )	( )
	Excellent	Very Good	Good	Satisfactory	Fair	Weak

Comment/Recommendations :

_____

_____

_____

_____

…… Name : ……

Signature and stamp of JKPP Chairman

Date : ……

b) RMC EVALUATION

Research Status	( )	( )	( )	( )	( )	( )
Spending	( )	( )	( )	( )	( )	( )
Overall Status	( )	( )	( )	( )	( )	( )
	Excellent	Very Good	Good	Satisfactory	Fair	Weak

Comments :-

_____

_____

_____

_____

_____

_____

Recommendations :

☐ Needs further research

☐ Patent application recommended

☐ Market without patent

☐ No tangible product. Report to be filed as reference

…….. Name : ……

Signature and Stamp of Dean / Deputy Dean
Research Management Centre

Date : ……